RESEARCH ARTICLE - HYDROLOGY AND HYDRAULICS

Development of PROMETHEE-Entropy data mining model for groundwater potentiality modeling: a case study of multifaceted geologic settings in south-western Nigeria

Kehinde Anthony Mogaji[1] · Olanrewaju Fred Atenidegbe[1,2]

Abstract

This work looks at developing an object-driven decision support system (DSS) model with the goal of improving the prediction accuracy of the present expert-driven DSS model in assessing groundwater potentiality. The database of remote sensing, geological, and geophysical information was constructed using the technological efficiency of GIS, data mining, and programming tools. Groundwater potential conditioning factors (GPCF) extracted from the datasets include lithology (Li), hydraulic conductivity (K), lineament density (Ld), transmissivity (T), and transverse resistance (TR) for groundwater potentiality mapping in a typical hard rock multifaceted geologic setting in south-western Nigeria. A Python-based entropy approach was used to objectively weight these factors. The weightage findings determined that the greatest and lowest given values for Ld and K were 0.6 and 0.03, respectively. The produced Python-based PROMETHEE-Entropy model algorithm was born through combining the weight findings with the Python-based PROMETHEE-II method. The groundwater potentiality model (GPM) map of the area was created using the model algorithm's outputs on the gridded raster of GPCF themes. Based on the suggested approach, the validated results of the created GPM maps using the Receiver Operating Characteristic (ROC) curve technique yielded an accuracy of 86%. An object-driven DSS model was created using the approaches that were used. The created object-driven model is a viable alternative to existing approaches in groundwater hydrology and aids in the automation of groundwater resource management in the research region.

Introduction

Water is an essential component of life since it maintains life (Akintorinwa et al. 2020). According to Arsene et al. (2018) and Srinivasan et al. (2013), these valuable but finite natural resources are generally required for home and industrial applications; without them, production and sustainability are near to impossible. Molden (2007) and Al Sabahi et al. (2009) define groundwater as water enclosed

in a geologic substance in the earth's subsurface known as an aquifer. These aquifer units might be weathered layers, voids, cracks, faults, and so forth. Groundwater is a major source of water in Nigeria for home use and agriculture. As a result, groundwater evaluation and acquisition are critical for obtaining portable drinking water, assisting in irrigation operations, and also in enterprises (Yousefi et al. 2018; Ouedraogo et al. 2016). According to Obaje (2009), groundwater occurrence in Nigeria's basement complex is relatively low and irregular, owing to the prevalence of abrupt discontinuities in features and faults responsible for groundwater accumulation, as well as low aquifer overburden (Olabode 2019; Anbazhagan et al. 2011; Chandra et al. 2008). Because of the nature of the crystalline basement rocks underlying the hard rock terrain, these discontinuities are frequently characterised by low porosity and low permeability of fluids percolation, which causes localisation of groundwater potential zones and scattered presence of

---

Edited by Dr. Michael Nones (CO-EDITOR-IN-CHIEF).

✉ Olanrewaju Fred Atenidegbe
ola00229@students.stir.ac.uk

1   Department of Applied Geophysics, Federal University of Technology, Akure, Nigeria

2   Present Address: Computing Science and Mathematics, University of Stirling, Stirling FK9 4LA, United Kingdom

pockets of groundwater accumulation present in the basement complex terrain, making groundwater occurrence generally low and irregular (Olabode 2019; Ajayi 2017; Akintorinwa 2014; Odeyemi et al. 1985). According to Ajayi (2017) and Mogaji et al. (2011), few crystalline rocks, such as schist, worn quartzite, gneiss, and so on, have exhibited great groundwater potential, and their aquifer units often serve as a conduit to the natural resource in huge quantities. Geophysical surveys are one of the most commonly used methodologies for evaluating groundwater potential zones since the conduit medium cannot be seen immediately on the earth's surface (Braga et al. 2006). Several researchers have done groundwater hydrology studies, particularly in hard rock terrain, with promising results, including Omosuyi (2010), Mogaji et al. (2014), Oladunjoye et al. (2019), and Akintorinwa et al. (2020).

In the realm of groundwater hydrology, the use of geographic information system (GIS) and remote sensing (RS) techniques has proven to be good in spatial analysis related hurdles (Mogaji et al. 2021; Rahmati and Meselle 2016; Rahmati et al. 2015; Manap et al. 2014; Nasiri et al. 2012). This is because satellite database archives provide convenient and rapid access to data, saving time and money in analysis (Zare et al. 2013). In prior study in this subject, the combined use of GIS, RS, and multicriteria decision analysis (MCDA) functioned as a superior decision support system in demarcating groundwater potential zones (Ajaykumar et al. 2020; Mogaji and Lim 2016; Al-Abadi 2015). MCDA approaches have been used to give weights to index parameters from various research (Arshad et al. 2020; Mogaji and Lim 2016; Adiat et al. 2012; Chowdhury et al. 2009). The Analytical Hierarchy Process is one of the most extensively utilised MCDAs (AHP). Based on fundamental mathematics and psychology, the AHP model is a systematic approach for organising and evaluating complicated decisions (Saaty 1987). It is a measuring theory based on pairwise comparisons that depends on expert opinion to establish priority scales. Yet, due to the model's subjectivity, the assessment may be inconsistent and prejudiced. Yet, it has been successfully applied in the subject of groundwater hydrology (Mogaji and Omobude 2017; Akinlalu et al. 2017; Adeyemo et al. 2017). Because of AHP's subjectivity and biases, academics have looked ahead and moved to research models that are devoid of human or expert input or viewpoints. They are also known as objective models or data-driven approach models. These models include frequency ratio (Arshad et al. 2020; Pourtaghi and Pourghasemi 2014; Elmahdy and Mohammed, 2014; Ozdemir 2011; Oh et al. 2011), artificial neural networks (Adiat et al. 2019; Lee et al. 2012; Corsini et al. 2009), weights of evidence (Chen et al. 2018; Pourtaghi and Pourghasemi 2014; Lee et al. 2012), maximum of entropy (Rahmati et al. 2015), preference ranking organisation method for enrichment evaluation

(PROMETHEE-II) (Widianta et al. 2018; Roodposhti et al. 2012), and evidential belief functions (Pourghasemi and Beheshtirad 2015; Nampak et al. 2014; Mogaji et al. 2014). These data-driven techniques employ mathematical algorithms with known well/spring locations as dependent variables, as well as other known factors, to assess groundwater occurrence in a certain geo-spatial setting (McKay and Harris 2015). The weights of the parameters evaluated for groundwater zonation of the research region were calculated using the entropy technique of weightage calculation in this study.

According to Lin and Weng (2009) and Wang et al. (2020), the entropy technique is an object (non-expert) driven strategy that comprises computing the entropy and entropy weight to determine the weight values of specific indicators. Entropy is inversely related to entropy weight, therefore the lower the entropy, the higher the associated entropy weight. The quantity of meaningful information provided by the target to the decision-maker is lowered. Many scholars in several branches of science have employed entropy extensively in the literature (Al-Abadi et al. 2017; Al-Abadi and Shahid 2016; Li et al. 2012; Safari et al. 2012; Qi et al. 2010).

Brans (1982) created the PROMETHEE-II algorithm, which was further upon by Vincke and Brans (1985). PROMETHEE-II employs a full ranking approach on a limited set of possibilities, ranging from best to worst. This approach compares options pairwise along each identified criterion and takes into account the preference function of criteria over others, which tends to provide superior results (Abdullah et al. 2019; Nasiri et al. 2012; Roodposhti et al. 2012). This approach has been widely employed in a variety of disciplines of study, including banking, water resource management, investments, healthcare, tourism, the industrial sector, dynamic management, and so on (Widianta et al. 2018; Roodposhti et al. 2012). This approach has been widely employed in a variety of disciplines of study, including banking, water resource management, investments, healthcare, tourism, the industrial sector, dynamic management, and so on (Widianta et al. 2018; Roodposhti et al. 2012).

The PROMETHEE-II approach based on entropy weight was employed in this study to assess the groundwater potentiality index and rating of the study region. The creation of these combined MCDA techniques was prompted by the combination of the properties of both model algorithms. To begin, the PROMETHEE-II considers the preference functions of each criteria to enhance decision-making regarding the outcome. Furthermore, the entropy technique employs a data-driven strategy in determining the weights of criteria, making this task object-driven and devoid of human input in producing the final algorithm index. Additionally, in the realm of groundwater hydrology, the coupling of these model techniques with GIS and RS has not been used to groundwater potential mapping. Lastly, because of its robust libraries

and high-speed computing capabilities, the model algorithms' procedures were calculated using the Python programming language (Butwall et al. 2019). These integrated methodologies were used to estimate the groundwater potentiality of the study region using geoelectrical and remote sensing-derived metrics such as lithology (L), hydraulic conductivity (K), lineament density (Ld), transmissivity (T), and transverse resistance (TR). The methodology was demonstrated in typical multifaceted geologic settings.

Methodology, study area, and data used

Methodology

As indicated in Fig. 1, the study technique was carried out in four stages, employing geology, remote sensing, and geophysical data. The initial phases required collecting, processing, and interpreting remote sensing, geology, and geophysical characteristics for this study's groundwater potential evaluation. Following that, thematic maps of the conditioning factors were created in ArcGIS, and uniformly spaced fishnet (observation) points were placed to extract pixel values at those points. Furthermore, the Python-based entropy method of weighting was used on the fishnet points, as well as the PROMETHEE-II algorithm, producing the PROMETHEE-Entropy-based groundwater potential index (GPI), which was synthesised in the GIS environment to produce the groundwater model map of the study area. Finally, the suggested model was validated using borehole data and a reflection coefficient map of the research region. Figure 1 depicts the process flowchart.

Fig. 1 The adopted methodology flowchart for the study
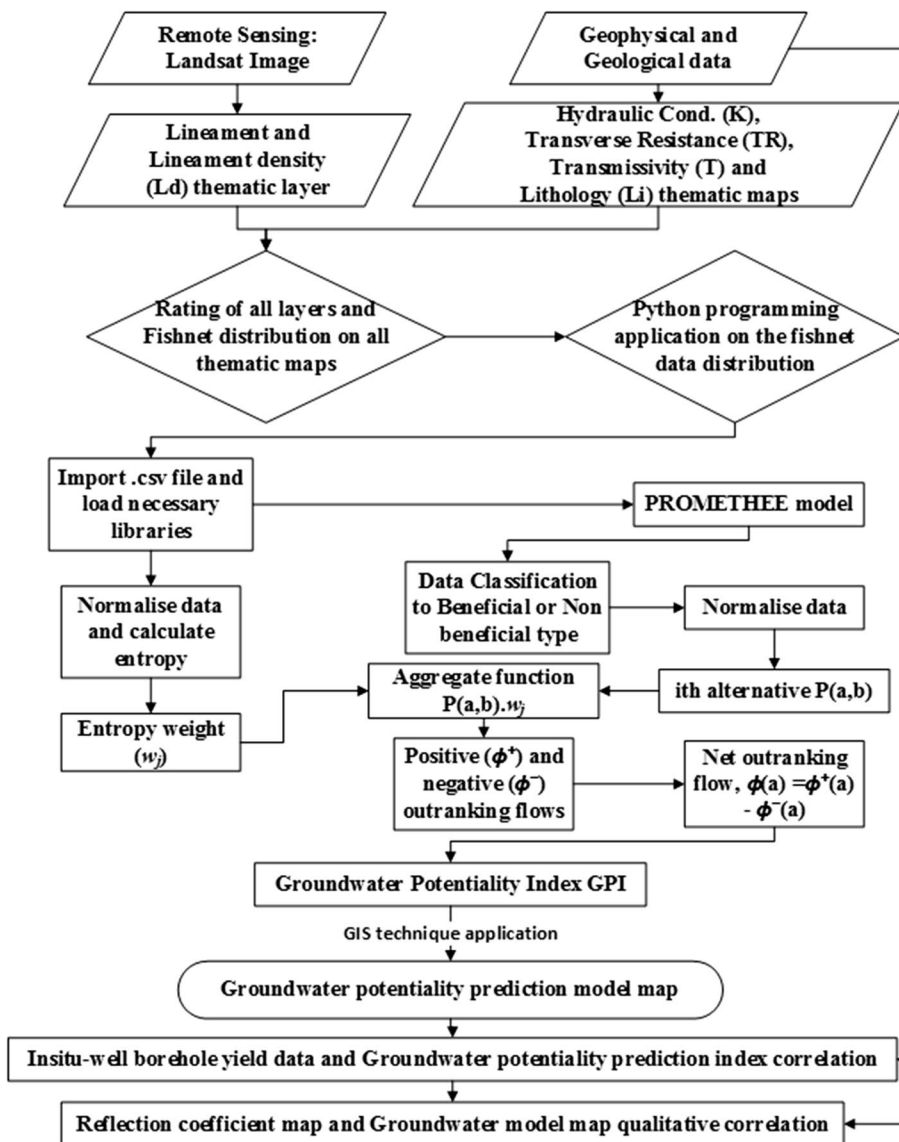
Description of the study area

The research area is in northern Ondo state, Nigeria, and includes the local government areas of Akoko south-west, Akoko south-east, Akoko north-west, Akoko north-east, and Ose, as indicated in Fig. 2. The region is designated by the Minna-Nigeria 31N datum of the UTM (Universal Traverse Mercatum) system and extends from longitude 5°30″E to 6°0″E and latitude 7°10″N to 7°45″N. It is surrounded to the west, north, and east by Ekiti, Kogi, and Benin states, respectively, and to the south by other sections of Ondo state. The overall area covered by the research area is approximately 1492.55 square kilometres. The terrain in the research region is relatively low to highly undulating, with surface elevations ranging from 162 to 1500 m above sea level. Ikare and Oke agbe, located in the northern half of the research region, have high elevations characteristic

of dispersed batholiths, but communities to the south, such as Idoani, Oba, and Idosale, have low-lying rock exposures (Olabode 2019; Oyedotun and Obatoyinbo 2012).

The environment is hot and humid, with rain-bearing south-west monsoon winds blowing in from the Sahara Desert. The rainy season lasts from April to October, with repeated maxima occurring from August to October, with annual rainfall ranging from 1500 to 2000 mm. The average annual temperature is roughly 23–26 °C (Duze and Ojo 1982), with a relative humidity of 75–95%. Forest-savannah vegetation is the natural vegetation.

The research area is underlain by the Precambrian basement complex of Southern Nigeria (Rahaman 1988). The geological units identified in the region include granite, migmatite gneiss, and quartzite. More than 70% of the area is underlain by migmatite gneiss. Figure 3 shows a geological map of the area.
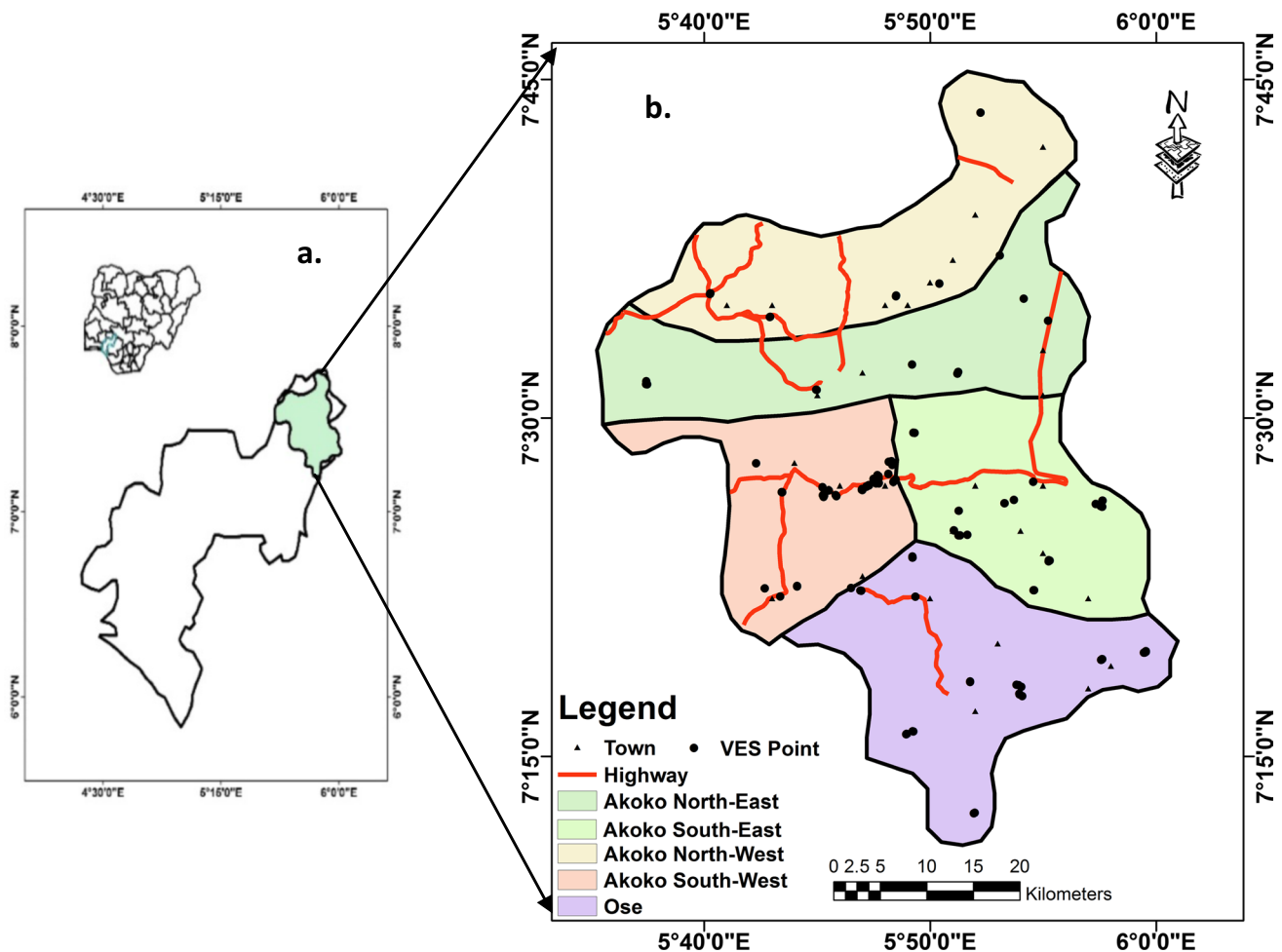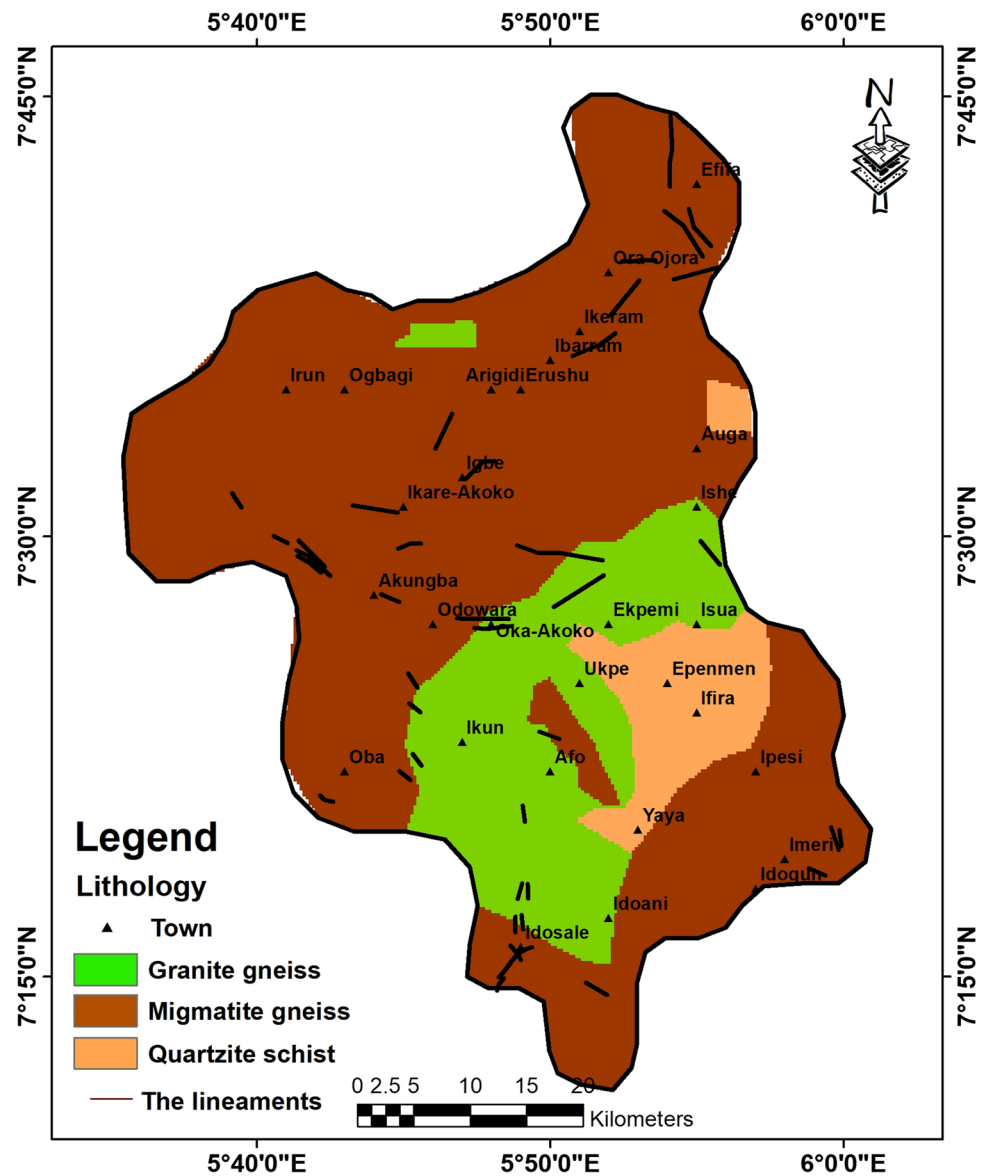

Fig. 2 Location maps showing: **a** map of Ondo State and Nigeria and **b** study area map displaying the data acquisition points and other features

Fig. 3 Geologic map of the study area (Modified after Geological and mineral resources map of Ondo State) Nigeria, 2006)

Data used

Lithology

The lithologic map of the research area was derived from Ondo State's regional geology and mineral resources map (NGSA 2006). After georeferencing the scanned copy of the regional map in an ArcGIS environment, the shape file of the research area was extracted from the state map to generate the lithological map of the study area shown in Fig. 3.

Remote sensing

The remote sensing techniques employed in this study include lineament extraction from LANDSAT 8 images of the subject region. In the year 2020, this image was retrieved

from the United States Geological Survey (USGS) Earth Explorer with route 189 and row 055. Visual interpretation of both LANDSAT 8 photos was used to identify the lineaments (Fig. 3). To extract the area of interest (AOI), a 432 (RGB) false-colour composite band combination was employed, followed by principal component analysis (PCA), band rationing, directional filtering, and edge enhancement using PCI Geomatica 2012. These lineaments were identified, photographed, scanned, and placed on a lithologic map (Fig. 3).

Lineaments are typically examined using frequency or length against azimuth histograms (Zakir et al. 1999; Mostafa and Zakir 1996), rose diagrams (Karnieli et al. 1996), and/or lineament density maps (Zakir et al. 1999; Mostafa and Zakir 1996). (Zakir et al. 1999). The most popular way is to construct density maps of lineaments

(Zakir et al. 1999). Equation (1) expresses the Ld definition mathematically:

$$Ld = \sum_{i=1}^{i=n} \frac{L_i}{A} \left(km^{-1} \right), \tag{1}$$

where $\sum L_i$ = total length of all the lineaments (km) and A = area of the grid (km^2).

The lineament density map is shown in Fig. 4 below.

Geophysical investigation

Data acquisition and interpretation The geophysical data in the study region were collected using the Schlumberger array of electrical resistivity techniques. The array was utilised to collect 118 vertical electrical soundings (VES) data from 1 to 100 m utilising half-electrode spacing (AB/2). This approach takes into account vertical differences in the apparent resistivity of the ground, which were measured with a fixed centre of the array. The survey was carried out by progressively expanding or increasing the electrode spacing around a fixed centre of the array. Normally, electrodes

Fig. 4 Lineament density thematic layer for the study area
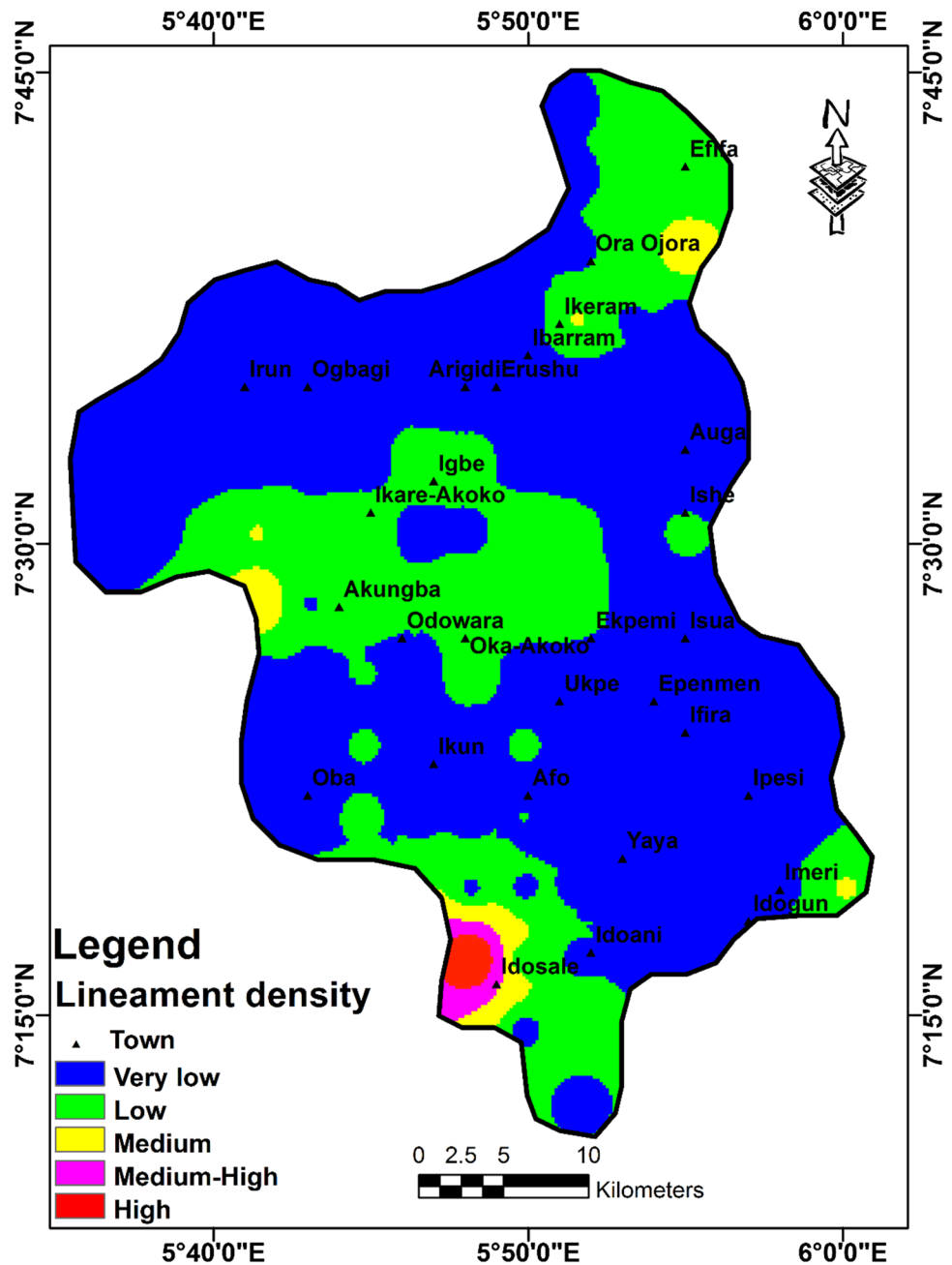
are positioned in a straight line, with a pair of potential electrodes placed between two pairs of current electrodes. In this work, the Global Positioning System (GPS) was utilised to spatially identify VES sites for spatial analysis in a GIS setting. The apparent resistivity of the VES data is the product of the resistance and the matching geometric factor (G) of the electrode spacing for each spread length (AB/2). On a log–log graph sheet, these apparent resistivity values were plotted against the electrode spacing. The VES curves that were generated were displayed and divided into types. These classifications demonstrate the qualitative character of subsurface lithology. In addition, quantitative interpretations of the partial curve matching findings, which are the layer thickness and layer resistivity, were determined. The results were entered into the WinResistTM Software as model parameters (Vander-Velper 2004). The theoretical model curve, the primary geoelectric parameters (layer resistivity, layer thickness), and the depth to the top of each layer provide good insight into the aquifer's subsurface information, which is vital for groundwater potential research. Figure 5 and Table 1 show typical curves depending on underlying geology and a summary table representation of geoelectric characteristics.

The derived secondary geoelectric parameter The primary geoelectric parameters, layer resistivity and layer thickness, were utilised to determine the secondary geoelectric parameters, which are important conditioning variables in delineating groundwater potential zones in the research region. The validation method takes into account hydraulic conductivity (K), transmissivity (T), transverse resistance (TR), and reflection coefficient (Rc). The primary geoelectric characteristics in Table 1 were reanalysed using Eqs. 2–5 to generate the aforementioned groundwater conditioning factors. Table 2 displays the values of the calculated K, T, TR, and Rc parameters.

Hydraulic conductivity, K (m/day), is given by:

$$K = 0.0538e^{-0.0072\rho}, \tag{2}$$

where ρ = aquifer resistivity

$$\text{Transmissivity}, T\left(\text{m}^2/\text{day}\right) = Kh, \tag{3}$$

where, K = hydraulic conductivity h = aquifer thickness

Transverse resistance, TR (Ωm)

$$= h_n * \rho_n = h_1 * \rho_1 + h_2 * \rho_2 + \ldots\ldots\ldots + h_n * \rho_n, \tag{4}$$
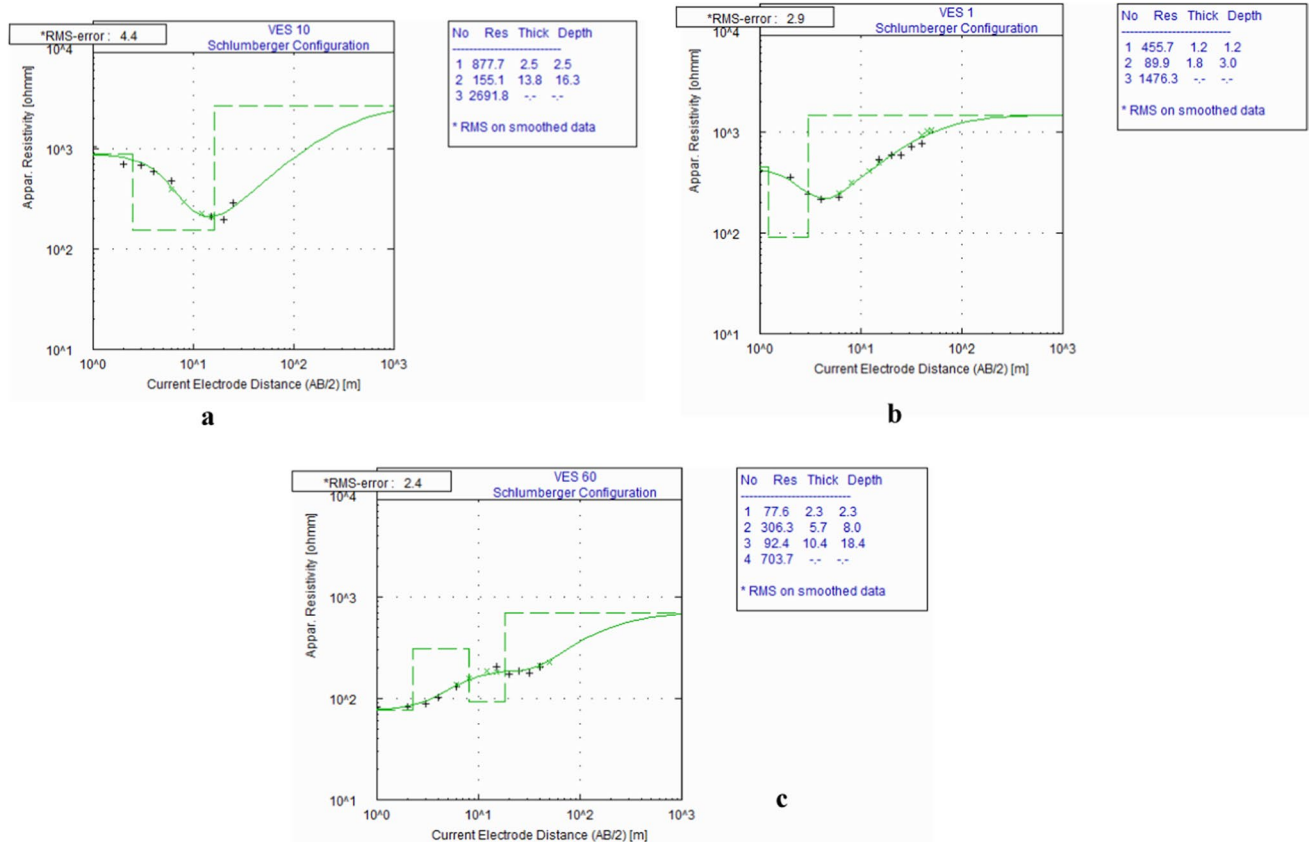

Fig. 5 Typical resistivity model curves obtained in the study area; **a** migmatite gneiss, **b** quartzite series and **c** granite gneiss rock unit

Table 1 Summary of the interpreted geoelectric parameters

VES	Layer resistivity (Ωm)					Layer thickness (m)				Curve type
	ρ_1	ρ_2	ρ_3	ρ_4	ρ_5	h_1	h_2	h_3	h_4	
1	456	90	1476			1.2	1.2			H
2	942	26	704			0.8	0.7			H
3	603	145	21196			0.8	3			H
4	2377	139	6065			0.4	6.2			H
5	1522	229	10615			1	14.8			H
6	1461	140	1429			0.7	2.8			H
7	1076	122	3124			0.7	2.4			H
8	426	122	658			0.3	5.4			H
9	1399	215	2322			0.9	1.9			H
10	878	155	2692			2.5	13.8			H
11	279	18	2557			0.7	0.4			H
12	4516	91	16224			1.2	12.2			H
13	4721	343	268	1191		1.3	0.4	14.3		QH
14	2060	357	5670			1.2	14.2			H
15	1208	171	3917			3.3	69			H
16	2277	480	1195	295	20096	1.1	1.5	6.1	10.6	HKH
17	525	77	2563			2	6.5			H
18	23	109	533			1	7.5			A
19	566	45	791	105	19560	0.5	0.5	4.5	15	HKH
20	101	254	137	6265		1.2	2.8	28		KH
21	53	130	80	203		1.1	2.9	5.4		KH
22	210	25	301	131	859	0.7	0.3	3.4	6.1	HKH
23	354	131	609			1.8	4.3			H
24	181	70	3633			1.1	1.6			H
25	147	309	20728			1.4	5.6			A
?	?					?				?
?	?					?				?
110	63	121	25	6776		0.8	1.6	3.4		KH
111	32	88	549			0.9	5			A
112	85	39	3523			1	2.6			H
113	64	30	2490			1.5	3.2			H
114	281	86	148	18315		0.6	1.1	4.4		HA
115	132	83	7708			0.8	3.2			H
116	255	641	192	15396		0.9	1.6	2.7		KH
117	404	71	1304			1	4			H
118	171	92	18785			1.6	3			H

where n = number of layers overlying the aquifer unit h = layer thickness, ρ = layer resistivity

$$\text{Reflection coefficient, Rc} = \frac{\rho_n - \rho_{n-1}}{\rho_n + \rho_{n-1}}, \quad (5)$$

where ρ_n is the layer resistivity of the nth layer and ρ_{n-1} is the layer resistivity overlying the nth layer.

Selection of groundwater potentiality conditioning factors (GPCF) and production of their thematic layers in the GIS environment The groundwater potential of the research was evaluated using five (5) factors: lithology, hydraulic conductivity, lineament density, transmissivity, and transverse resistance. Thematic maps of these factors were generated using ArcGIS 10.3's inverse distance weighting (IDW) approach, and data from Table 2 were utilised to develop the geo-electrically linked thematic layers displayed in Figs. 6, 7, and 8.

Table 2 Summary of the derived secondary geoelectric parameters

| VES	Lat	Long	K (m/day)	T (m²/day)	TR (Ωm)	Rc
1	7.3726	5.782	0.028142	0.033771	548.2	0.885057
2	7.3724	5.7825	0.044615	0.031231	754.6	0.928767
3	7.4453	5.7239	0.01894	0.05682	483.4	0.986411
4	7.4452	5.72416	0.019776	0.122612	951.8	0.95519
5	7.44521	5.72424	0.010345	0.153101	1523	0.957765
6	7.37594	5.73524	0.019634	0.054976	1023.7	0.821542
7	7.37552	5.73532	0.022351	0.053643	754.2	0.924831
8	7.58986	5.8083	0.022351	0.120696	128.8	0.687179
9	7.59042	5.808326	0.011442	0.021739	1260.1	0.830508
10	7.59928	5.840215	0.017624	0.243214	2196	0.891113
11	7.588169	5.902494	0.04726	0.018904	196.3	0.986019
12	7.619999	5.884966	0.02794	0.340873	5420.2	0.988845
13	7.725406	5.87069	0.007812	0.111713	6275.5	0.632625
14	7.725434	5.87069	0.004116	0.058447	2473	0.881533
15	7.374188	5.7116	0.015706	1.083747	3987.4	0.916341
16	7.37413	5.711435	0.006432	0.068178	4425.8	0.971066
17	7.37452	5.775158	0.030904	0.200874	1051	0.941667
18	7.57175	5.92052	0.024544	0.184081	24	0.660436
19	7.539312	5.820104	0.025261	0.378919	1101	0.989321
20	7.52084	5.749325	0.020063	0.561762	833.4	0.957201
21	7.520675	5.74963	0.030243	0.163314	436.3	0.434629
22	7.5207	5.74966	0.020949	0.127787	458.9	0.735354
23	7.304917	5.86299	0.020949	0.090079	638.2	0.645946
24	7.305333	5.86291	0.032501	0.052002	200.1	0.962193
25	7.396825	5.82033	0.005815	0.032565	206.8	0.970623
?	?	?	?	?	?	?
?	?	?	?	?	?	?
110	7.26853	5.820464	0.044938	0.152788	245	0.992648
111	7.26834	5.82108	0.02855	0.142752	29.8	0.723705
112	7.326942	5.992162	0.040629	0.105634	86	0.978102
113	7.326692	5.99169	0.043349	0.138715	97	0.97619
114	7.326637	5.99108	0.018535	0.081555	264.2	0.983968
115	7.3278	5.9926	0.029597	0.09471	106.6	0.978693
116	7.327165	5.992634	0.013502	0.036457	1256.1	0.975366
117	7.574587	5.71538	0.032268	0.129072	405	0.896727
118	7.574559	5.715157	0.02774	0.08322	274.6	0.990253

K: Hydraulic conductivity; TR: Transverse resistance; T: Transmissivity; Rc: Reflection coefficient

The groundwater potential conditioning factors (GPCF) thematic maps shown in Figs. 2, 4, 6, 7, and 8 were created to model the groundwater potential of the research region. These layers were used as input parameters for developing the suggested PROMETHEE-Entropy model method in Python. Table 3 was created for ease of computation by guaranteeing uniformly dispersed fishnet points (Fig. 9) over the study area. Akintorinwa et al. (2020), Olabode 2019, Alhassan et al. (2015), and Nasiri et al. (2012) have highlighted the hydrological relevance of the GPCF for the suggested model method (2012).

Models review

The entropy method According to Lin and Weng (2009), the entropy method is an object-driven (non-expert) significance approach that involves determining the weight values of individual indicators by calculating the entropy and entropy weight (Qi et al. 2010). The method is based on the idea of discreet probability distribution where uncertainty is depicted with broad distribution (Zou et al. 2006) and since entropy is the measure of a system's disorder nature, it can be used to extract useful information from a given data (Al-Abadi et al. 2016). The difference in the values of the evalu-

**Fig. 6** Hydraulic conductivity map of the study area
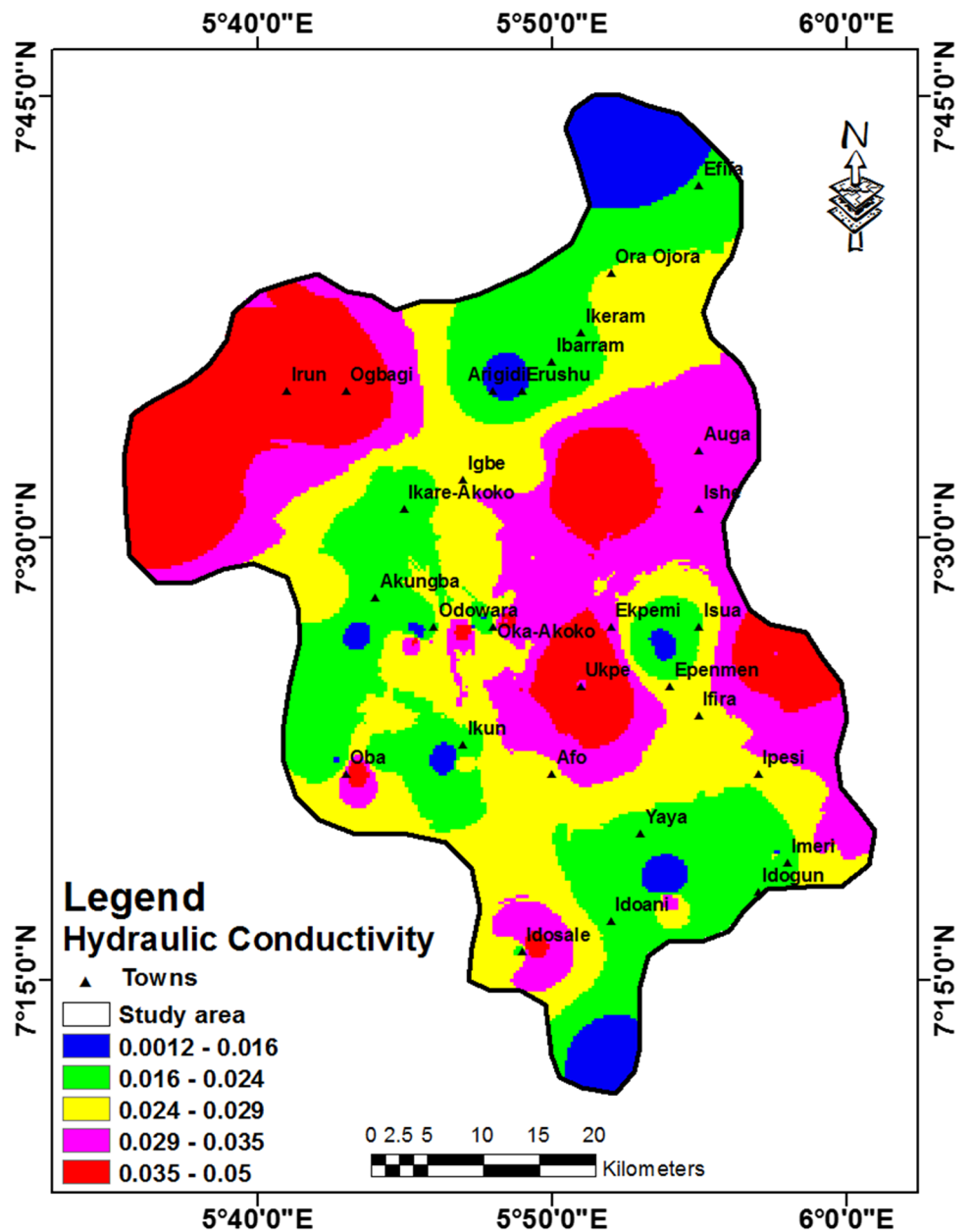
ating objects on a criteria has a direct effect on the entropy, which is inversely proportional to the entropy weight. Many scholars in several branches of science have employed entropy extensively in the literature (Al-Abadi et al. 2017; Al-Abadi and Shahid 2016; Li et al. 2012; Safari et al. 2012; Qi et al. 2010).

Shannon proposed the notion of the index of entropy first (1948). The approach allows us to calculate the weights by assuming that the issue has m viable alternatives, A_i (i = 1,2,…,m), and n assessment criteria C_j (j = 1,2,…,n) (Aysegul and Esra 2017). The first step is to create the choice

matrix (Eq. 6). The essence is that it compares the performance of several alternatives based on many parameters.

$$X = (Xij)_{m \times n} = \begin{pmatrix} X_{11} & X_{12} & \dots & X_{1n} \\ & & . & \\ & & . & \\ & & . & \\ X_{2n} & X_{2n} & \dots & X_{2n} \\ & & . & \\ & & . & \\ & & . & \\ X_{m1} & X_{m2} & \dots & X_{mn} \end{pmatrix} \quad (6)$$

Fig. 7 Transmissivity map of the study area
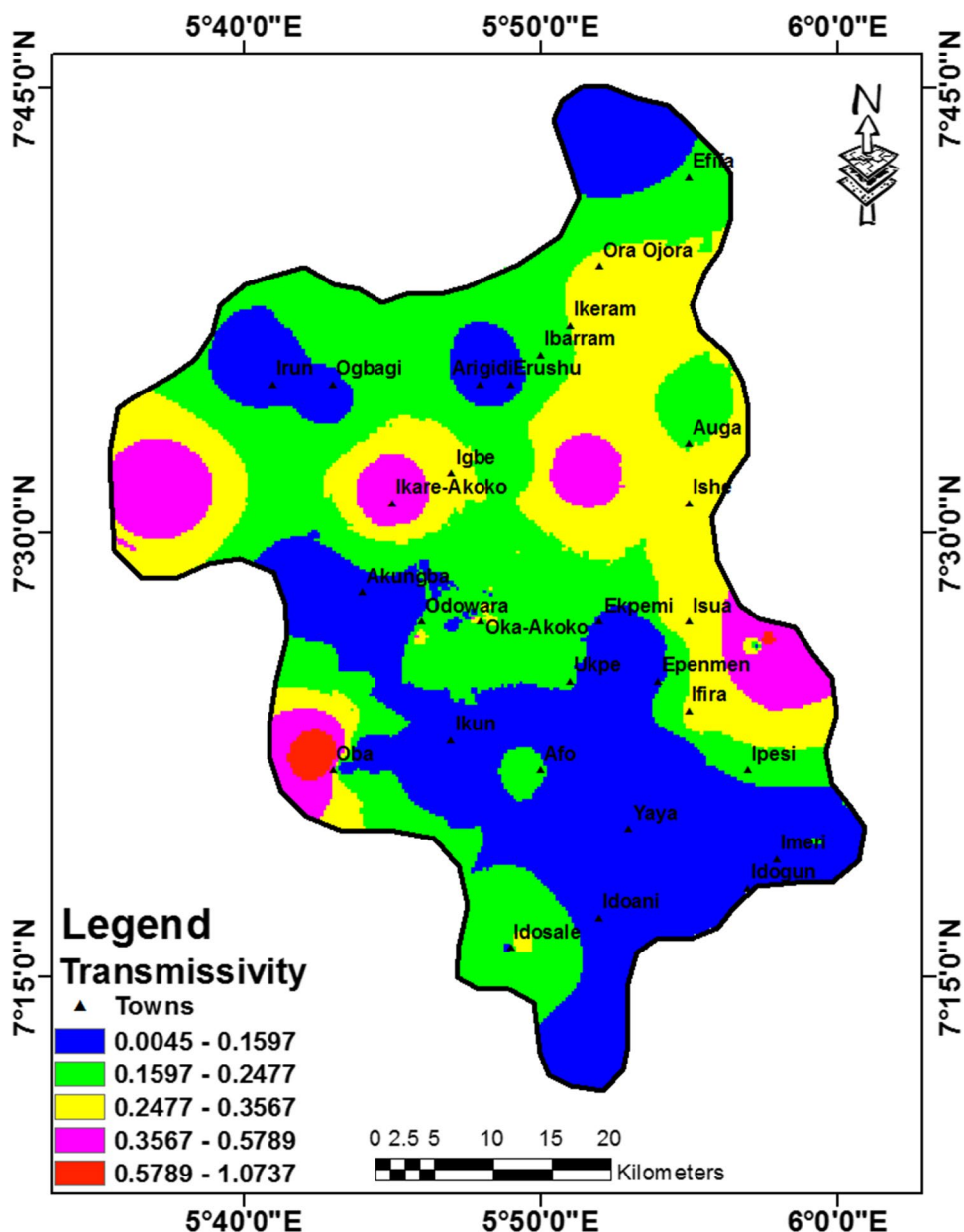
for $i = 1, 2 \ldots, m$; $j = 1, 2, \ldots, n$, where X_{im} = feasible alternatives, X_{jn} = evaluation criteria, m = number of alternatives, n = number of criteria

After the preceding steps, the decision matrix is normalised by dividing each criterion value (X_{ij}) by the total arithmetic column sum of the criteria. The normalised equation is written as Eq. (7):

$$r_{ij} = \frac{x_{ij}}{\sum_{i=1}^{m} x_{ij}} i = 1, 2 \ldots, m; j = 1, 2, \ldots, n. \tag{7}$$

The entropy values of each criterion are then calculated. After the above stages, the entropy values (e_j) (as in Eq. 8) are computed.
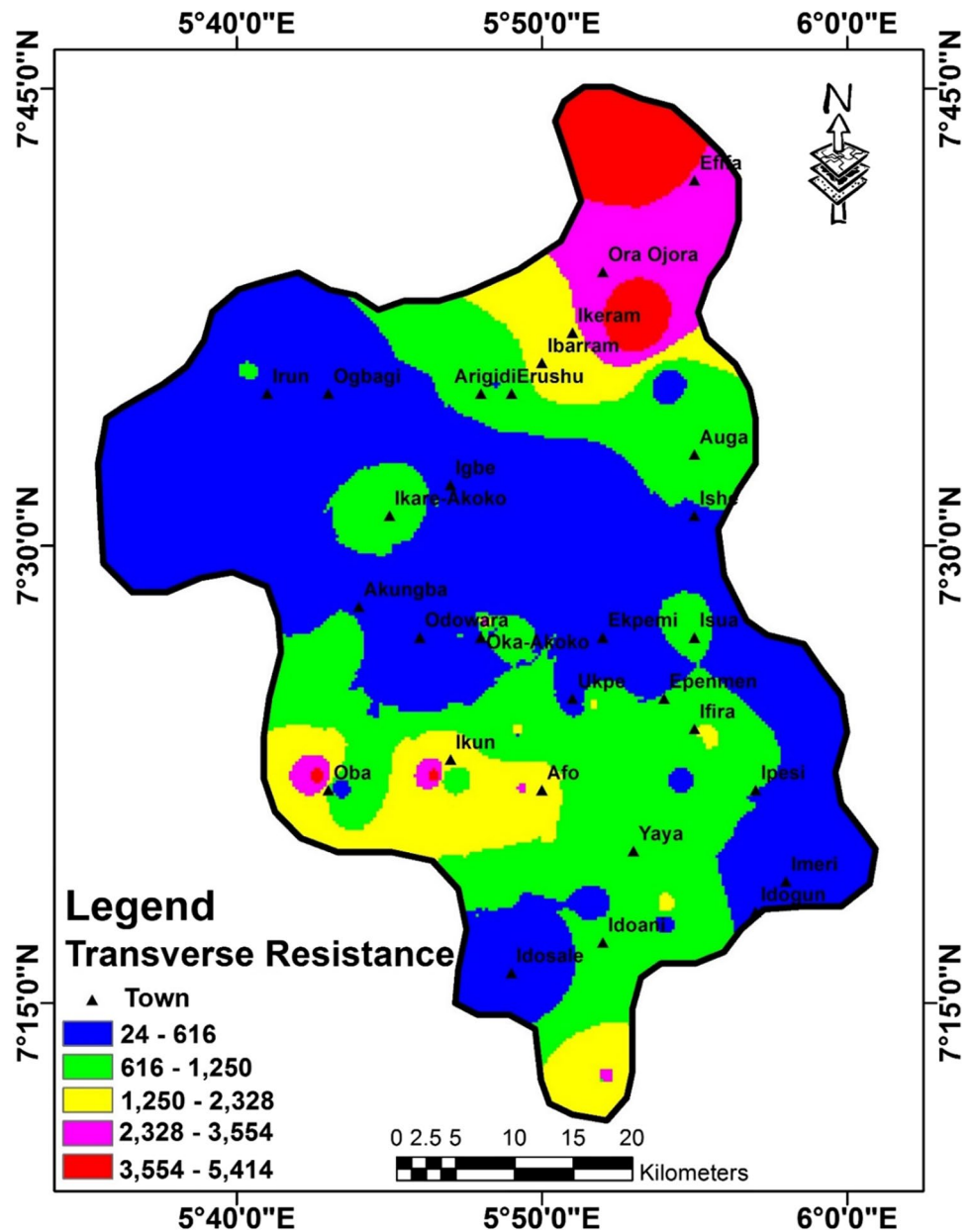
$$e_j = -h \sum_{i=1}^{m} r_{ij} \in r_{ij} \text{ i } = 1, 2 \ldots, m; j = 1, 2, \ldots, n, \tag{8}$$

where $h = \frac{1}{m}$.

Then entropy weight (w_j), Eq. 9, is calculated:

$$w_j = \frac{1 - e_j}{n - \sum_{i=1}^{m} e_j}, \tag{9}$$

Fig. 8 Transverse resistance map of the study area

where $\sum_{j=1}^{n} w_j = 1.$ (10)

Entropy Python class The entropy weights for each groundwater potential conditioning factor (GPCF) studied in this study were computed using a Python programming class attribute. After embedding the Python-based entropy function into a class property, the appropriate libraries were imported, input variables were assigned, and the table was imported as a csv file. The normalised weights of the GPCFs computed using the Python-based entropy weight-

ing approach are shown in Table 4. The entropy technique codes are presented in the Appendix.

PROMETHEE-II The PROMETHEE-II technique is a comprehensive outranking flow method created by Brans (1982) and later extended by Vincke and Brans (1985). This approach is one of the PROMETHEE methods created to help decision-makers rate a finite number of choices partially or entirely (Nasiri et al. 2012; Roodposhti et al. 2012). The preference function of each criterion versus other criteria is considered, resulting in a smooth and robust decision-making process when employing PROMETHEE-II (Nasiri et al. 2012).

Table 3 Decision matrix for the groundwater potential conditioning factors

Fishnet no	Longitude	Latitude	L	K (m/day)	Ld (km^2)	T (m^2/day)	TR (Ωm)
0	5.859741	7.204569	17	0.009	0.02	0.088	3022
1	5.831421	7.242249	17	0.029	0.02	0.196	601
2	5.859741	7.242249	17	0.023	0.13	0.145	1111
3	5.803101	7.279928	17	0.03	0.78	0.206	422
4	5.831421	7.279928	29	0.033	0.13	0.224	328
5	5.859741	7.279928	29	0.024	0.02	0.14	588
6	5.888062	7.279928	17	0.023	0.02	0.098	605
7	5.916382	7.279928	17	0.023	0.02	0.095	623
8	5.803101	7.317607	29	0.027	0.04	0.151	870
9	5.831421	7.317607	29	0.025	0.04	0.147	759
10	5.859741	7.317607	29	0.022	0.02	0.123	535
11	5.888062	7.317607	17	0.016	0.02	0.072	685
12	5.916382	7.317607	17	0.019	0.02	0.078	640
13	5.944702	7.317607	17	0.023	0.02	0.105	388
14	5.973022	7.317607	17	0.025	0.07	0.122	320
15	6.001343	7.317607	17	0.03	0.33	0.143	265
16	5.689819	7.355286	17	0.026	0.04	0.458	1141
17	5.71814	7.355286	17	0.032	0.06	0.317	779
18	5.74646	7.355286	17	0.026	0.12	0.192	1123
19	5.77478	7.355286	29	0.022	0.02	0.112	1629
20	5.803101	7.355286	29	0.027	0.02	0.126	1544
21	5.831421	7.355286	29	0.028	0.08	0.159	1728
22	5.859741	7.355286	17	0.028	0.02	0.115	870
23	5.888062	7.355286	54	0.026	0.02	0.114	688
24	5.916382	7.355286	17	0.024	0.02	0.112	529
25	5.944702	7.355286	17	0.024	0.02	0.123	525
26	5.973022	7.355286	17	0.029	0.02	0.155	349
27	5.689819	7.392965	17	0.024	0.02	0.415	996
28	5.71814	7.392965	17	0.024	0.02	0.372	1078
29	5.74646	7.392965	17	0.025	0.1	0.187	976
30	5.77478	7.392965	29	0.023	0.02	0.107	1433
31	5.803101	7.392965	29	0.03	0.02	0.114	829
32	5.831421	7.392965	17	0.034	0.11	0.105	601
33	5.859741	7.392965	29	0.039	0.02	0.127	764
34	5.888062	7.392965	54	0.031	0.02	0.14	748
35	5.916382	7.392965	54	0.028	0.02	0.266	1647
36	5.944702	7.392965	54	0.03	0.02	0.285	808
37	5.973022	7.392965	17	0.033	0.02	0.321	407
38	5.689819	7.430644	17	0.023	0.02	0.173	709
39	5.71814	7.430644	17	0.02	0.02	0.168	857
40	5.74646	7.430644	17	0.028	0.09	0.145	372
41	5.77478	7.430644	17	0.029	0.02	0.186	304
42	5.803101	7.430644	29	0.029	0.17	0.198	385
43	5.831421	7.430644	29	0.037	0.02	0.195	607
44	5.859741	7.430644	54	0.043	0.02	0.159	285
45	5.888062	7.430644	54	0.019	0.02	0.1	392
46	5.916382	7.430644	54	0.025	0.02	0.243	580
47	5.944702	7.430644	54	0.039	0.02	0.377	273
48	5.973022	7.430644	17	0.038	0.02	0.489	255
49	5.689819	7.468323	17	0.026	0.57	0.092	380
50	5.71814	7.468323	17	0.024	0.07	0.111	482

Table 3 (continued)

Fishnet no	Longitude	Latitude	L	K (m/day)	Ld (km^2)	T (m^2/day)	TR (Ωm)
51	5.74646	7.468323	17	0.023	0.1	0.137	412
52	5.77478	7.468323	17	0.025	0.08	0.154	241
53	5.803101	7.468323	17	0.033	0.18	0.212	335
54	5.831421	7.468323	29	0.032	0.11	0.222	509
55	5.859741	7.468323	29	0.03	0.22	0.172	374
56	5.888062	7.468323	29	0.026	0.02	0.194	476
57	5.916382	7.468323	29	0.026	0.04	0.288	567
58	5.604858	7.506002	17	0.039	0.02	0.383	280
59	5.633179	7.506002	17	0.039	0.02	0.391	266
60	5.661499	7.506002	17	0.033	0.09	0.256	432
61	5.689819	7.506002	17	0.027	0.32	0.186	485
62	5.71814	7.506002	17	0.024	0.1	0.215	521
63	5.74646	7.506002	17	0.022	0.24	0.397	674
64	5.77478	7.506002	17	0.027	0.02	0.269	369
65	5.803101	7.506002	17	0.03	0.03	0.21	328
66	5.831421	7.506002	17	0.033	0.25	0.251	240
67	5.859741	7.506002	17	0.038	0.12	0.316	219
68	5.888062	7.506002	29	0.034	0.02	0.296	350
69	5.916382	7.506002	29	0.032	0.12	0.324	400
70	5.604858	7.543681	17	0.04	0.02	0.385	294
71	5.633179	7.543681	17	0.04	0.02	0.391	289
72	5.661499	7.543681	17	0.035	0.02	0.257	487
73	5.689819	7.543681	17	0.034	0.02	0.206	487
74	5.71814	7.543681	17	0.03	0.02	0.237	491
75	5.74646	7.543681	17	0.026	0.02	0.362	591
76	5.77478	7.543681	17	0.028	0.17	0.309	451
77	5.803101	7.543681	17	0.028	0.14	0.232	257
78	5.831421	7.543681	17	0.031	0.02	0.251	176
79	5.859741	7.543681	17	0.044	0.02	0.42	303
80	5.888062	7.543681	17	0.036	0.02	0.315	644
81	5.916382	7.543681	17	0.032	0.02	0.273	857
82	5.944702	7.543681	17	0.032	0.02	0.298	863
83	5.633179	7.58136	17	0.036	0.02	0.207	720
84	5.661499	7.58136	17	0.039	0.02	0.142	1011
85	5.689819	7.58136	17	0.039	0.02	0.151	715
86	5.71814	7.58136	17	0.042	0.02	0.147	163
87	5.74646	7.58136	17	0.034	0.02	0.201	462
88	5.77478	7.58136	17	0.025	0.07	0.191	837
89	5.803101	7.58136	17	0.015	0.02	0.064	1182
90	5.831421	7.58136	17	0.022	0.02	0.21	1203
91	5.859741	7.58136	17	0.027	0.02	0.274	1246
92	5.888062	7.58136	17	0.031	0.02	0.277	1389
93	5.916382	7.58136	17	0.031	0.02	0.216	1115
94	5.944702	7.58136	54	0.032	0.02	0.257	1115
95	5.661499	7.619039	17	0.037	0.02	0.157	899
96	5.689819	7.619039	17	0.037	0.02	0.17	786
97	5.71814	7.619039	17	0.036	0.02	0.197	653
98	5.74646	7.619039	17	0.032	0.02	0.214	741
99	5.77478	7.619039	29	0.025	0.02	0.186	1027
100	5.803101	7.619039	17	0.02	0.02	0.165	1225
101	5.831421	7.619039	17	0.021	0.02	0.22	1467

Table 3 (continued)

Fishnet no	Longitude	Latitude	L	K (m/day)	Ld (km^2)	T (m^2/day)	TR (Ωm)
102	5.859741	7.619039	17	0.025	0.33	0.275	2102
103	5.888062	7.619039	17	0.028	0.05	0.339	3370
104	5.916382	7.619039	17	0.028	0.02	0.281	2137
105	5.831421	7.656718	17	0.023	0.02	0.223	1571
106	5.859741	7.656718	17	0.024	0.02	0.245	1944
107	5.888062	7.656718	17	0.025	0.25	0.264	2211
108	5.916382	7.656718	17	0.025	0.52	0.262	2020
109	5.859741	7.694397	17	0.014	0.02	0.14	2093
110	5.888062	7.694397	17	0.015	0.17	0.151	2102
111	5.916382	7.694397	17	0.019	0.18	0.19	1932
112	5.859741	7.732076	17	0.006	0.02	0.07	2413
113	5.888062	7.732076	17	0.007	0.22	0.083	2346

L: Lithology; K: Hydraulic conductivity; Ld: Lineament density; T: Transmissivity; TR: Transverse resistance

PROMETHEE-II is based on a pairwise analysis of options for each criterion. The procedure consists of four phases, which are highlighted below.

Determination of deviations based on pairwise comparisons by computing the desired degree value for each pair of possible decisions and each criterion is stated in Eq. (11). The preference function is used in the way shown in Eq. (12):

$$d_j(a, b) = g_j(a) + g_j(b) \tag{11}$$

$$P_j(a, b) = F_j\big[d_j(a, b)\big] j = 1, \ldots, k, \tag{12}$$

where $g_j(a)$ and $g_j(b)$ show the performance (value of a criterion j) of alternatives a and b (for a decision a or decision b), respectively. $d_j(a,b)$ = difference of the performance (value of a criterion j for two decisions a and b).

$P_j(a, b)$ is the preference of alternative a regarding alternative b on each criterion, as a function of $d_j(a, b)$.

Aggregation of all criteria's preference degrees for each pair of potential options, followed by computation of the global preference index for each of these possible decisions, is indicated in Eq. (13):

$$\forall a, b \in A, \ \pi(a, b) = \sum_{j=1}^{k} P_j(a, b) w_j, \tag{13}$$

where $\pi(a, b)$ is the preference of an over b (from zero to one) and w_j is the weight associated with jth criterion.

Calculation of the outranking flows (positive and negative outranking flow) is shown in Eqs. 14 and 15.

$$\phi^{\mp}(a) = \frac{1}{n-1} \sum_{x \in A} \Pi(a, x) \tag{14}$$

$$\phi^-(a) = \frac{1}{n-1} \sum_{x \in A} \Pi(x, a), \tag{15}$$

where $\phi^+(a)$ and $\phi^-(a)$ are positive and negative outranking flows for each alternative, respectively.

Calculation of complete outranking flow index is shown in Eq. 6.

$$\phi(\text{a}) = \phi^+(\text{a}) - \phi^-(\text{a}), \tag{16}$$

where $\phi(a)$ is the net outranking flow for each alternative.

PROMETHEE-II Python class In this study, the PROMETHEE-II steps were implemented utilising the class feature of the Python programming language. The constructor, which initialises the class object, and the net outranking flow method are included in the Python PROMETHEE-II class. The class feature was activated when the required libraries were imported. The following Python programmes were used to compute the PROMETHEE-net II's outranking flow.

Preparation of the proposed PROMETHEE-Entropy model for groundwater potential mapping

The object-oriented prowess of the PROMETHEE-Entropy algorithm was a key consideration in this study, which was accomplished by modelling five groundwater potential conditioning factors (GPCFs): lithology (L), hydraulic conductivity (K), lineament density (Ld), transmissivity (T), and transverse resistance (TR). The number of criteria (GPCF), number of alternatives (fishnet points), weights of each criterion, and types of criteria were among the input parameters utilised in constructing the Python-based PROMETHEE-Entropy algorithm. The algorithm procedures are divided
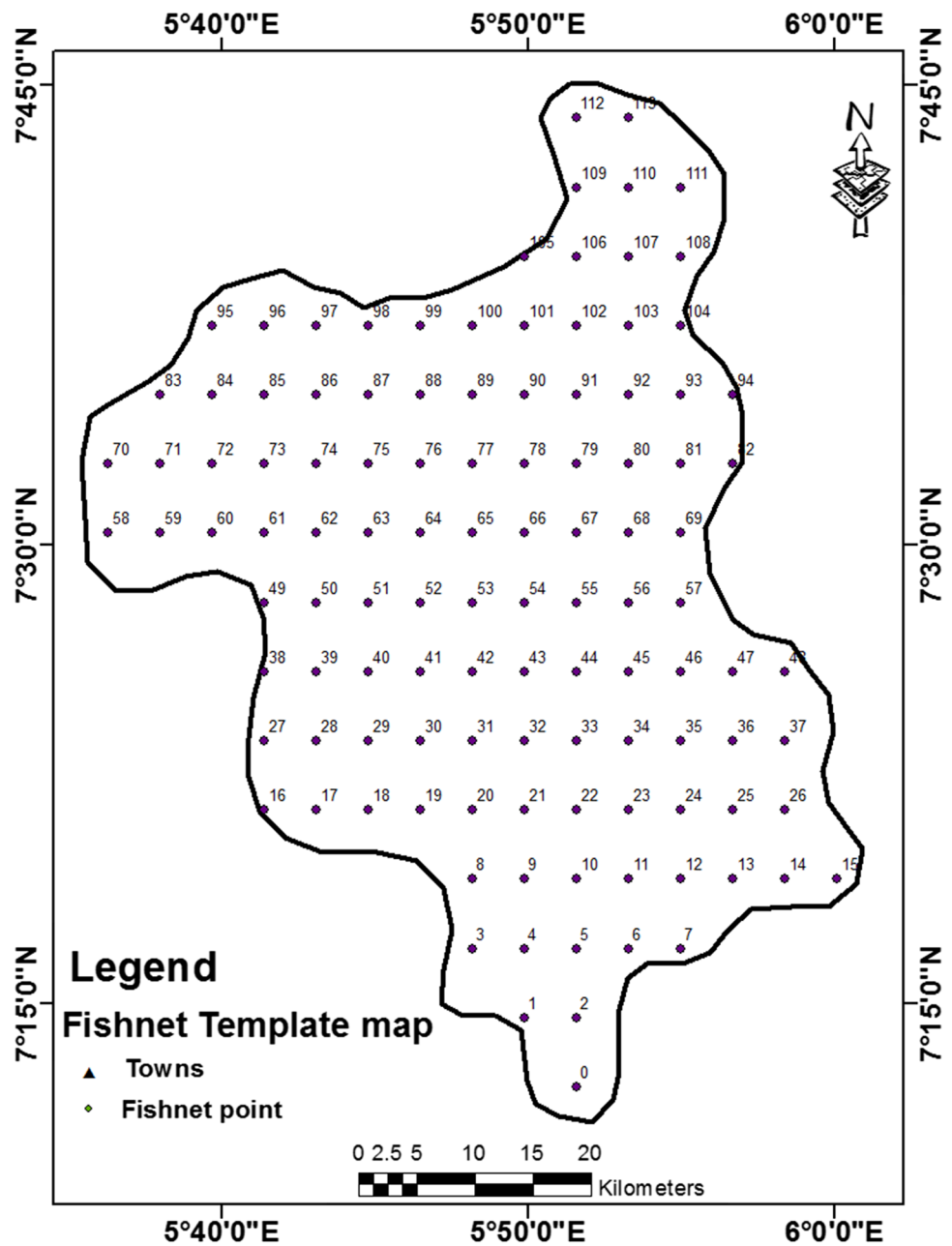
Fig. 9 Fishnet template map of the study area

Table 4 Calculated entropy values, degree of divergence and entropy weights for groundwater potential conditioning factors

	L	K	Ld	T	TR
Entropy values (e_j)	0.981412	0.992321	0.847570	0.980040	0.950980
$d_j (1 - e_j)$	0.018588	0.007679	0.152430	0.019960	0.049020
Entropy weights (w_j)	0.075501	0.03006	0.61476	0.080599	0.199090

L: Lithology; K: Hydraulic conductivity; Ld: Lineament density; T: Transmissivity; TR: Transverse resistance

into two phases. The first is the computation of the objective weights of each criterion using the entropy approach, which was accomplished using the previously stated Python-based entropy algorithms. These weights were then supplied into

the PROMETHEE-II class along with other input parameters. The criteria were divided into two types: beneficial and non-beneficial criteria, denoted numerically by 1 and −1, respectively. (Table 5). Beneficial criteria are those in

Table 5 Ratings, groundwater storage potential type-classification and entropy weight of the GPCF produced thematic layers

GPCFs thematic maps	Classes	Potential of groundwater storage	Type	Entropy weight (w_j)
Lithology	Migmatite Gneiss: 17	Low	Beneficial: 1	0.0755
	Granite Gneiss: 29	Medium		
	Quartzite Schist: 54	High		
Hydraulic conductivity	0.0012–0.016	Very low	Beneficial: 1	0.03006
	0.016–0.024	Low		
	0.024–0.029	Medium		
	0.029–0.035	Medium–high		
	0.035–0.5	High		
Lineament density	0.02–0.074	Very low	Beneficial: 1	0.61476
	0.074–0.2996	Low		
	0.2996–0.8558	Medium		
	0.8558–1.73	Medium–high		
	1.73–3.155	High		
Transmissivity	0.0045–0.1597	Very low	Beneficial: 1	0.0806
	0.1597–0.2477	Low		
	0.2477–0.3567	Medium		
	0.3567–0.5789	Medium–high		
	0.5789–1.0737	High		
Transverse resistance	24–616	Very low	Beneficial: 1	0.19909
	616–1250	Low		
	1250–2328	Medium		
	2328–3554	Medium–high		
	3554–5414	High		

which the maximum values are preferred, whereas non-beneficial criteria are those in which the minimum values are preferred. The net outranking flow index of this study was calculated using the combined Python-based entropy and PROMETHEE-II classes.

Results and discussion

Discussion of groundwater potential conditioning factors

As shown in column 3 of Table 5, groundwater potential conditioning factors (GPCFs) have a significant importance to groundwater accumulation in the aquifer. The relevance is discussed further below.

Lithology

Lithology is a significant component that affects groundwater accumulation in an ecosystem, particularly in terms of quantity. There are three primary geological units in the research area: Migmatite gneiss, Granitic gneiss, and Quartzite Schist (Fig. 3). As compared to other rock groups in the study region, Quartzite Schist exhibits the greatest degree of fracture (Olabode 2019). The amount and potential of groundwater in the research region is directly related to the degree of weathering of the rocks in the study area. Olabode (2019) assigned the following values to each of the lithologic units in Table 3: magmatite gneiss (17), granite gneiss (29), and quartzite schist (57). For migmatite, granite, and quartzite, the area extents are 1096.91, 108.54, and 287.1 km² correspondingly. The Migmatite gneiss rock unit covers over 75% of the study region. The majority of the towns in the north, north-central, and north-west are underlain by Migmatite gneiss rock units, whereas the centre and southern parts of the study region are underlain by Quartzite Schist rock units, and the south-east is underlain by Granite gneiss rock units.

Lineament density

Lineament is defined as observable geomorphic linear features typified by weak zones with characteristics of fissures/joints, fractures, and possibly weathered formation that can be attributed to geological structures, most notably fractures

or lithologic contacts (Chowdhury et al. 2009 and O'Leary et al. 1976). The distribution of lineament (Fig. 4) and density of lineament (Fig. 5) demonstrate that over 95% of the research region is underlain by lineament at a very low to low density. As a result, the region may be classified as having low to medium groundwater potential. Nevertheless, the zones with significant groundwater potential in the studied region are attributable to secondary porosity and permeability, which are also characterised by high lineament density (Olabode 2019). According to the lineament density map (Fig. 5), the geographical distribution of the lineament density of the study region is separated into five zones (very low, low, medium, medium–high, and high), with area extents of 965.25, 484.05, 25.25, 9.05, and 8.95 km² correspondingly.

Hydraulic conductivity

This refers to an aquifer's physical capacity to transfer water through pore spaces and cracks when subjected to a hydraulic gradient (Diminescu et al. 2019). According to Table 3, the hydraulic conductivity, K, of the research region varies from 0.5 to 12.5 m/day. The resulting thematic map (Fig. 7) depicts the regional variance of hydraulic conductivity in the research area. The area extend coverage of the categorised zones is 38.55, 387.25, 428.25, 324.25, and 268.25 km² correspondingly. According to Okogbue and Omonona (2013), Lee et al. (2012), and Tizro et al. (2010), groundwater potentiality is directly related to an aquifer's K rating. The K parameter greatly influences the variability of groundwater potential from location to location. According to the areal extent computation, about 68% of the research area is underlain by medium to high hydraulic conductivity zones, whereas 32% is inhabited by relatively low and low hydraulic conductivity zones. It implies that the aquifer units in the area have a high groundwater potential in general. Unfortunately, the K parameter cannot alone confirm this assessment of the area's groundwater potential.

Transmissivity

The ability of water to pass through pores spaces of a unit width of the aquifer under a unit hydraulic gradient is referred to as aquifer transmissivity (Salem 1999). This means that aquifer units with high transmissivity have high fluid permeability across their pore spaces. The transmissivity of the research region ranges from 0.02 to 33.3 m³/day, as shown in Table 3. The resulting aquifer Transmissivity map (Fig. 8) depicts the geographical variance of the research area's transmissivity, which is divided into five zones: very low, low, medium, medium–high, and high. According to the characteristic shown in Fig. 8, the research region has

typically poor transmissivity, with low groundwater potential zones covering almost 71% of the area. Many communities in Akoko's south-west, east, and north-west, including Ora Ojora, Ikeram, Yaya, Ishe, Isua, Igbe, Ikare-Akoko, and Oba, are within the medium to high transmissivity zones.

Traverse resistance

Figure 9 depicts the total transverse resistance of the research region, which varies spatially from 24 to 5414 m (Table 3). Figure 9 depicts the generated TR map, which is divided into five zones (high, medium–high, medium, low, and very low zones). According to the produced thematic map, Akoko north-east and north-west have primarily low transverse resistance, which might be suggestive of possibly low groundwater potential zones in the area, whereas towns like Ikarram, Ijora, and Efifa may be experiencing the reverse. This situation of low transverse resistance also applies to other places where towns such as Oba, Ikun, and Afo are expected to face a mixed destiny due to limited groundwater potential. This submission is consistent with the findings of Adiat et al. (2012), who found that high transverse resistance indicates high permeability of water through the aquifer's overlaying strata, implying that TR is directly proportional to an area's groundwater potential.

The PROMETHEE-Entropy index application results

The data-driven ability of the suggested PROMETHEE-Entropy algorithm to get an object-oriented output is the primary emphasis of this work, which was accomplished by following the flowchart methodology in Fig. 1. The initial step is to extract the fishnet point pixel values from each GPCF (Table 3). This table functioned as the decision matrix for the following phase of the process, which required determining the entropy weightage. Table 4 shows the weights of each GPCF after passing the matrix through the Python-based entropy weight class. Table 5 displays the ratings, classifications, criterion type, and potential of GPCFs values to groundwater potential. The details from Tables 4 and 5 were used as input into the PROMETHEE-II class to compute the PROMETHEE-Entropy index, and the implementation codes are presented in the Appendix.

Table 6 displays the resultant data frame from above, and higher values indicate fishnet sites with more groundwater potential, while lower index values indicate fishnet points with lower groundwater potential.

Table 6 Computed model results of PROMETHEE-Entropy class algorithms

Fishnet no	Longitude	Latitude	Positive outranking flow	Negative outranking flow	Net outranking flow
0	5.859741	7.204569	0.13649	0.09411	0.04238
1	5.831421	7.242249	0.014206	0.086833	−0.07263
2	5.859741	7.242249	0.09459	0.060055	0.034535
3	5.803101	7.279928	0.58728	0.048207	0.539073
4	5.831421	7.279928	0.097911	0.064619	0.033292
5	5.859741	7.279928	0.026535	0.089977	−0.06344
6	5.888062	7.279928	0.007136	0.10305	−0.09591
7	5.916382	7.279928	0.007639	0.102999	−0.09536
8	5.803101	7.317607	0.048521	0.073482	−0.02496
9	5.831421	7.317607	0.043248	0.077522	−0.03427
10	5.859741	7.317607	0.024179	0.095788	−0.07161
11	5.888062	7.317607	0.008925	0.110387	−0.10146
12	5.916382	7.317607	0.007647	0.108386	−0.10074
13	5.944702	7.317607	0.002434	0.110598	−0.10816
14	5.973022	7.317607	0.02998	0.096753	−0.06677
15	6.001343	7.317607	0.219726	0.069763	0.149963
16	5.689819	7.355286	0.087055	0.061808	0.025247
17	5.71814	7.355286	0.05984	0.063134	−0.00329
18	5.74646	7.355286	0.09248	0.053969	0.038512
19	5.77478	7.355286	0.072961	0.078158	−0.0052
20	5.803101	7.355286	0.06998	0.073833	−0.00385
21	5.831421	7.355286	0.115548	0.051802	0.063746
22	5.859741	7.355286	0.01845	0.090525	−0.07208
23	5.888062	7.355286	0.076605	0.085697	−0.00909
24	5.916382	7.355286	0.005561	0.102758	−0.0972
25	5.944702	7.355286	0.005803	0.101146	−0.09534
26	5.973022	7.355286	0.005811	0.102065	−0.09625
27	5.689819	7.392965	0.061171	0.071149	−0.00998
28	5.71814	7.392965	0.057146	0.070215	−0.01307
29	5.74646	7.392965	0.071953	0.060723	0.01123
30	5.77478	7.392965	0.062465	0.080096	−0.01763
31	5.803101	7.392965	0.036068	0.084604	−0.04854
32	5.831421	7.392965	0.063958	0.076563	−0.0126
33	5.859741	7.392965	0.039702	0.082641	−0.04294
34	5.888062	7.392965	0.081835	0.078206	0.003629
35	5.916382	7.392965	0.136403	0.054756	0.081647
36	5.944702	7.392965	0.098889	0.064558	0.034331
37	5.973022	7.392965	0.028941	0.086612	−0.05767
38	5.689819	7.430644	0.013867	0.088917	−0.07505
39	5.71814	7.430644	0.018836	0.087968	−0.06913
40	5.74646	7.430644	0.044578	0.084979	−0.0404
41	5.77478	7.430644	0.007675	0.100816	−0.09314
42	5.803101	7.430644	0.121633	0.060294	0.061339
43	5.831421	7.430644	0.037472	0.07883	−0.04136
44	5.859741	7.430644	0.08061	0.092769	−0.01216
45	5.888062	7.430644	0.067869	0.103762	−0.03589
46	5.916382	7.430644	0.083348	0.075321	0.008027
47	5.944702	7.430644	0.106955	0.081349	0.025606
48	5.973022	7.430644	0.0612	0.09226	−0.03106
49	5.689819	7.468323	0.408714	0.068644	0.340069

Table 6 (continued)

Fishnet no	Longitude	Latitude	Positive out-ranking flow	Negative out-ranking flow	Net outranking flow
50	5.71814	7.468323	0.031936	0.091465	− 0.05953
51	5.74646	7.468323	0.049609	0.084864	− 0.03526
52	5.77478	7.468323	0.036935	0.094373	− 0.05744
53	5.803101	7.468323	0.113398	0.065864	0.047534
54	5.831421	7.468323	0.086743	0.059617	0.027127
55	5.859741	7.468323	0.15649	0.059214	0.097276
56	5.888062	7.468323	0.028152	0.086681	− 0.05853
57	5.916382	7.468323	0.052779	0.071303	− 0.01852
58	5.604858	7.506002	0.042229	0.091205	− 0.04898
59	5.633179	7.506002	0.043589	0.091912	− 0.04832
60	5.661499	7.506002	0.058962	0.07038	− 0.01142
61	5.689819	7.506002	0.216589	0.055175	0.161414
62	5.71814	7.506002	0.058113	0.07082	− 0.01271
63	5.74646	7.506002	0.189971	0.045623	0.144348
64	5.77478	7.506002	0.017297	0.092083	− 0.07479
65	5.803101	7.506002	0.015884	0.093972	− 0.07809
66	5.831421	7.506002	0.16967	0.063501	0.106169
67	5.859741	7.506002	0.088617	0.073425	0.015192
68	5.888062	7.506002	0.043166	0.083689	− 0.04052
69	5.916382	7.506002	0.105924	0.057949	0.047975
70	5.604858	7.543681	0.04344	0.090359	− 0.04692
71	5.633179	7.543681	0.044482	0.090566	− 0.04608
72	5.661499	7.543681	0.021941	0.085251	− 0.06331
73	5.689819	7.543681	0.015073	0.088939	− 0.07387
74	5.71814	7.543681	0.016502	0.087377	− 0.07087
75	5.74646	7.543681	0.036737	0.080625	− 0.04389
76	5.77478	7.543681	0.118771	0.057564	0.061208
77	5.803101	7.543681	0.084354	0.07451	0.009844
78	5.831421	7.543681	0.015545	0.102671	− 0.08713
79	5.859741	7.543681	0.053067	0.089535	− 0.03647
80	5.888062	7.543681	0.035606	0.077188	-− 0.04158
81	5.916382	7.543681	0.034288	0.073757	− 0.03947
82	5.944702	7.543681	0.038374	0.072684	− 0.03431
83	5.633179	7.58136	0.02322	0.080706	− 0.05749
84	5.661499	7.58136	0.032321	0.081625	− 0.0493
85	5.689819	7.58136	0.02062	0.086739	− 0.06612
86	5.71814	7.58136	0.012986	0.112049	− 0.09906
87	5.74646	7.58136	0.014066	0.090453	− 0.07639
88	5.77478	7.58136	0.04804	0.069233	− 0.02119
89	5.803101	7.58136	0.030184	0.102847	− 0.07266
90	5.831421	7.58136	0.038624	0.076455	− 0.03783
91	5.859741	7.58136	0.050173	0.069077	− 0.0189
92	5.888062	7.58136	0.059817	0.066	− 0.00618
93	5.916382	7.58136	0.037935	0.072949	− 0.03501
94	5.944702	7.58136	0.109424	0.059627	0.049797
95	5.661499	7.619039	0.02681	0.081853	− 0.05504
96	5.689819	7.619039	0.023103	0.082737	− 0.05963
97	5.71814	7.619039	0.019976	0.083571	− 0.0636
98	5.74646	7.619039	0.02218	0.080202	− 0.05802
99	5.77478	7.619039	0.046841	0.07319	− 0.02635

Table 6 (continued)

Fishnet no	Longitude	Latitude	Positive out-ranking flow	Negative out-ranking flow	Net outranking flow
100	5.803101	7.619039	0.035644	0.082302	− 0.04666
101	5.831421	7.619039	0.053322	0.073503	− 0.02018
102	5.859741	7.619039	0.311349	0.02507	0.286279
103	5.888062	7.619039	0.201797	0.04996	0.151836
104	5.916382	7.619039	0.100542	0.061506	0.039036
105	5.831421	7.656718	0.059443	0.070941	− 0.0115
106	5.859741	7.656718	0.083099	0.066229	0.01687
107	5.888062	7.656718	0.254357	0.02864	0.225717
108	5.916382	7.656718	0.455724	0.022018	0.433706
109	5.859741	7.694397	0.081246	0.083111	− 0.00187
110	5.888062	7.694397	0.175937	0.051928	0.124009
111	5.916382	7.694397	0.176496	0.044321	0.132175
112	5.859741	7.732076	0.09887	0.100469	− 0.0016
113	5.888062	7.732076	0.225144	0.064443	0.1607

Table 7 Characteristics of the groundwater potentiality model (GPM) map based on PROMETHEE-Entropy model

Groundwater potential classification	Areal extent (km^2)	Percentage coverage (%)
Very Low (VL)	539.09	30
Low (L)	366.64	42
Medium (M)	240.75	18
Medium–High (MH)	233.06	8
High (H)	113.01	2

Groundwater potential PROMETHEE-Entropy model map of the study area

The PROMETHEE-Entropy method, which is written in Python, produced the net outranking flow (groundwater potential index), as shown in Table 6 column 6. The groundwater potential model map of the study area was generated using the computed net outranking flow. The map obtained using the index is shown in Fig. 11. Using the Natural Breaks Method, the generated map was divided into five (5) groundwater potential zones (Jenks 1967). The study area's geographic variation of the groundwater potential index is split into five zones: extremely low, low, medium, medium–high, and high. According to a further analysis of the generated GPM, the area extents of the very low, low, medium, medium–high, and high classes are 442.1, 629.1, 273.5, 122.5, and 25.35 km^2, respectively (Table 7). The chart shows that the majority of the towns in the Akoko north-east and north-west lie within the very low to low groundwater potential zones, with the exception of a few towns in the north-eastern section of the study, which include Ikeram, Efifa, and Ora-Ojora. Furthermore, the majority of the remaining areas of the research fell mostly within the extremely low to low groundwater potential zones.

Validation of model

The PROMETHEE-Entropy GPM map was validated by two means: qualitative and quantitative. The resulting GPM map was qualitatively confirmed using accessible

Table 8 The groundwater potentiality model map validation result based on in situ borehole yield data

BH	Longitude	Latitude	Actual Yield from drilled borehole (m^3/h)	Actual yield description	Expected yield description from PROMETHEE-Entropy model map	Remark
1	5.905689	7.680997	1.23	Medium–High	Medium High	Coincide
2	5.720119	7.534097	2.36	Medium–High	Low	Not coincide
3	5.742189	7.478507	0.59	Very low–Low	Low	Coincide
4	5.742182	7.467231	0.7	Very low–Low	Low	Coincide
5	5.694379	7.434255	1.1	Medium–High	Very low	Not coincide
6	5.815618	7.443087	1.67	Medium–High	Medium	Coincide
7	5.873525	7.485179	0.83	Very low–Low	Low	Coincide

Fig. 10 The groundwater potentiality model (GPM) map of the study area based on PROMETHEE-Entropy approach
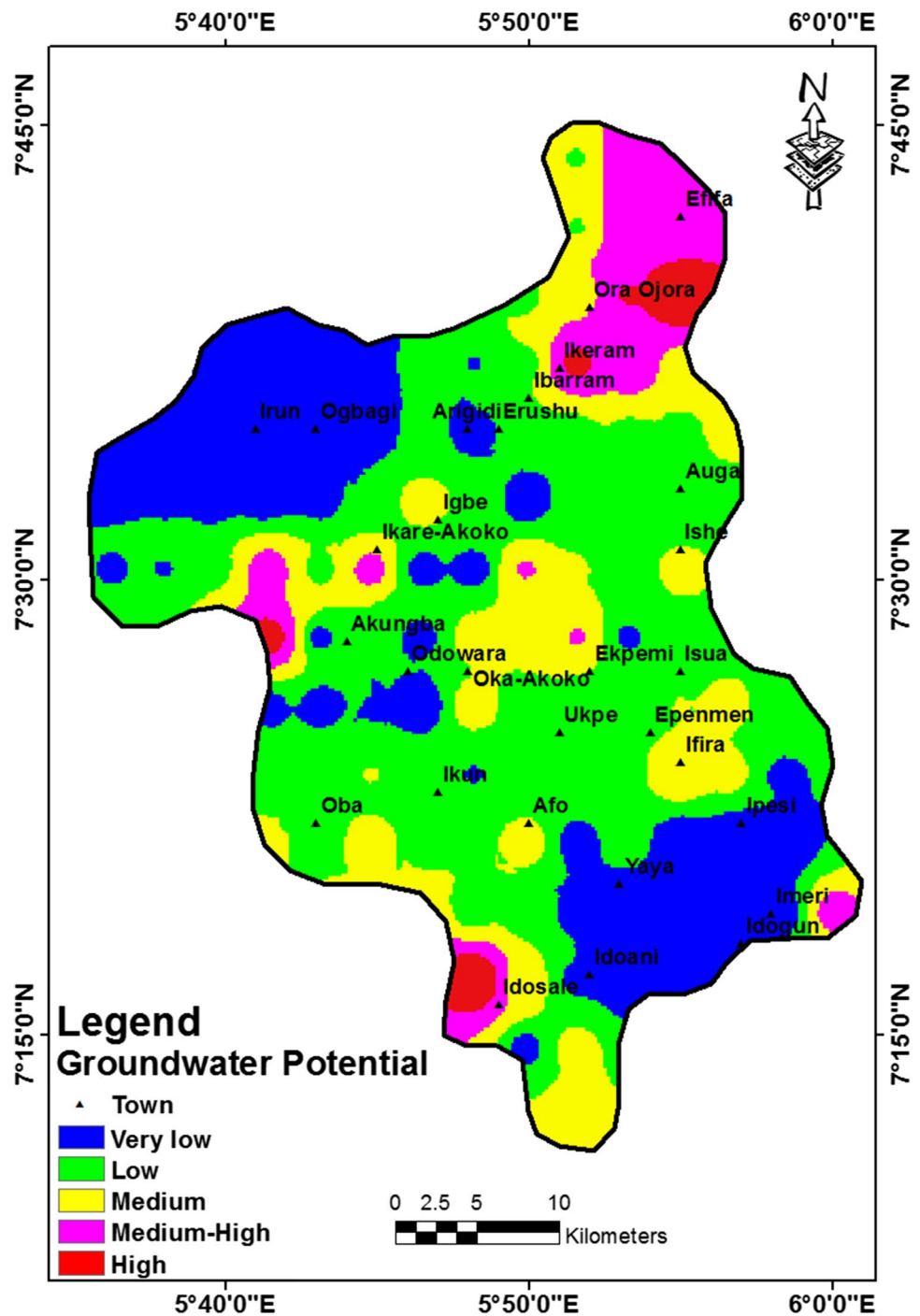
records of borewell yield data from the study area. The Ondo State Water and Sanitation Department provided these scanty borehole yield statistics (WATSAN). According to Mogaji (2016), the area actual yield descriptions of 0.2 l/s, > 0.2 l/s, 1 l/s, > 1 l/s, 1.5 l/s, and > 2 l/s are for the very low rate, low rate, medium rate, and high rate, respectively (Table 8). These were utilised to assess the prediction maps' percentage accuracy, which is based on the comment of coincide and not coincide between

the predicted yield descriptions from the prediction map (Fig. 10) and the actual borehole yields descriptions. This analysis is as follows:

Total number of boreholes available = 7.

Number of boreholes where the expected and the actual yield classifications coincide = 5

Number of boreholes where the expected and the actual yield classifications do not coincide = 2

Success rate (accuracy) of the prediction $= \frac{5}{7} \times 100 = 71\%$

Fig. 11 Reflection coefficient map of the study area
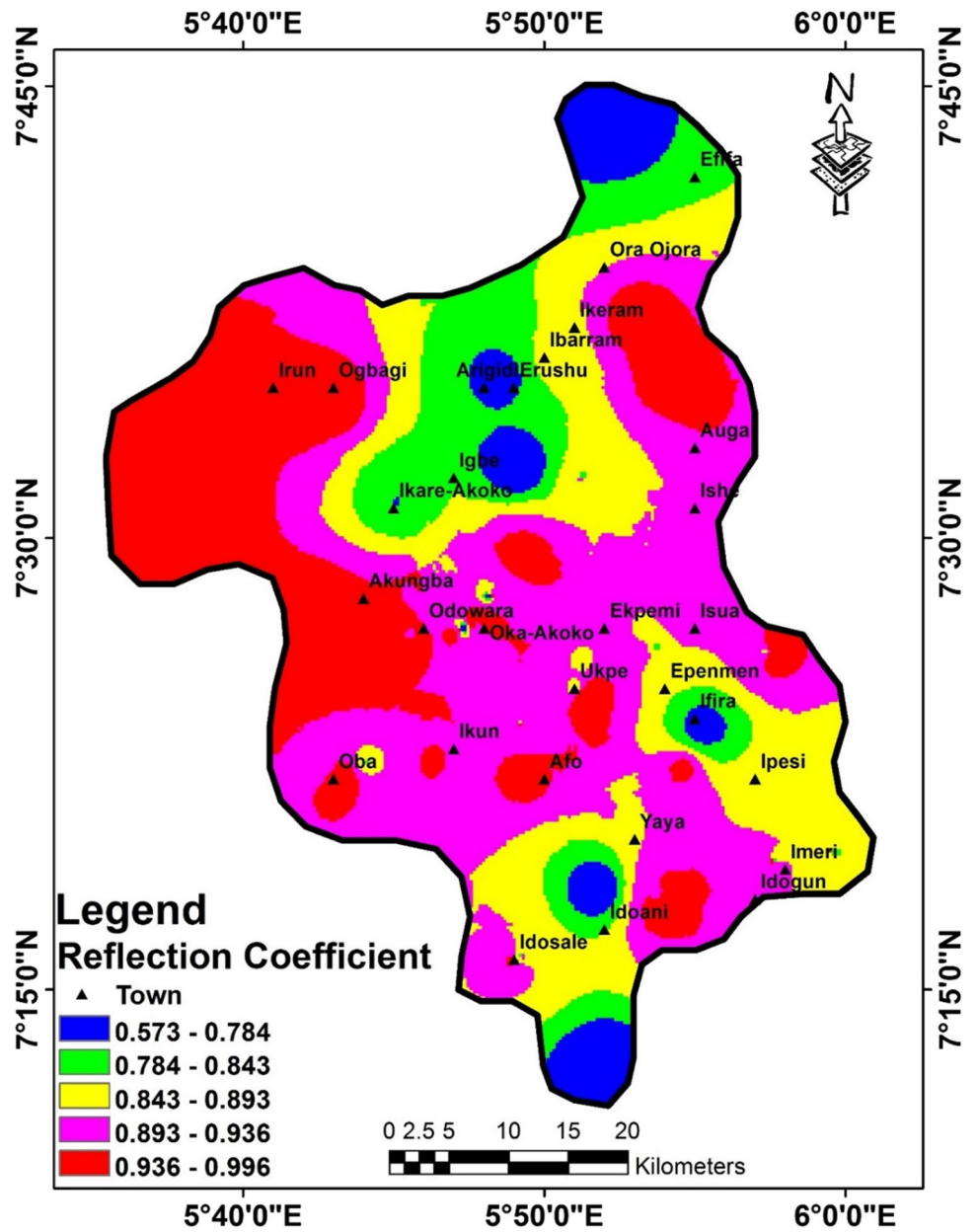
Table 9 Confusion Matrix application in generating the ROC curves

Actual values	Predicted values	
Cut-point	High potential (1)	Low potential (0)
High potential (1)	True positive(TP)	False positive(FP)
Low potential (0)	False negative(FN)	True negative

Table 10 Groundwater Potential cut-off points

Groundwater model map class	Cut-off points
Very low	0.2
Low	0.4
Medium	0.6
Medium–high	0.8
High	1.0

The quantitative validation, on the other hand, was carried out using the Reacting Operating Characteristics (ROC) curve technique, in which the confusion matrix (ROC) was applied to the actual data, i.e. the derived Reflection coefficient parameter, and the predicted data (Groundwater potential index, GPI) of the study area. The reflection coefficient (Rc), Fig. 11, parameter as a groundwater potentiality indicator is significant because it provides an in situ evaluation of the rate of fracture that an area bedrock has undergone. This Rc feature, according to Ariyo et al. (2011) and Alhassan et al. (2015), will frequently improve aquifer unit rechargeability through the fracture conduit medium and therefore enable groundwater accumulation. The AUC (Area under the curve) of the PROMETHEE-Entropy GPM index map was calculated using the ROC confusion matrix. The True Positive Rate (TPR) and False Positive Rate (FPR) were calculated for the determined Reflection coefficient parameter values of the study area, as shown in Table 9, by first marking the cut-off points on the GPM map index (Table 10) and binary (True (1) or False (0)) cut-off points, with values between 0.5 and 0.87 as True and 0.87 and 0.99 as False (Table 2). The predicted groundwater potential index (GPI) values were extracted from the GPM map at various cut-points and compared with the actual reflection coefficient (Rc) values using Table 9 criteria. The Rc values were compared to the appropriate GPI values to calculate the True Positive (TP), False Positive (FP), True Negative (TN), and False Negative (FN). Equations 17 and 18 were used to get the TPR (Sensitivity) and FPR (1-Specificity). The area under the curve (AUC) was computed after the ROC curve (Fig. 12) was displayed using the relevant Python libraries. The AUC value indicates the accuracy of the PROMETHEE-Entropy groundwater potential map.

$$\text{Sensitivity} = \text{TPR} = \frac{FP}{(TN + FP)} \tag{17}$$

$$1 - \text{Specificity} = \text{FPR} = \frac{TP}{(FN + TP)} \tag{18}$$

The AUC value of the prediction rate for the PROMETHEE-Entropy-based model is 0.86 prediction accuracy based on the findings of this investigation, as shown in Fig. 12. According to Naghibi et al. (2014), the following AUC classes correspond to the prediction accuracy of each model map as reported: 0.9–1.0 (excellent), 0.8–0.9 (very good), 0.7–0.8 (good), 0.6–0.7 (average), and 0.5–0.6 (poor). Given the categorisation above, it is possible to infer that the PROMETHEE-Entropy-based model performs "very good."

Conclusion

The use of object-driven multicriteria decision analysis (MCDA) techniques on geophysical, geological, ancillary, and remote sensing parameters in establishing groundwater resource sustainability management in typical hard rock geologic settings in south-western Nigeria was investigated in this study. The object-oriented PROMETHEE-Entropy MCDA approach was applied to 114 fishnet (observation) points distributed over the study area's generated thematic maps. Thematic maps have been generated by using GIS on processed data from Schlumberger VES data, remote sensing, and auxiliary data. The Python programming language was utilised to compute the model algorithms employed in this study for ease of calculation.

Fig. 12 ROC curve for the PROMETHEE-Entropy model map

This is due to Python's flexibility and high-level computational skills as a result of the existence of vast libraries and other resources.

The groundwater potential conditioning factors (GPCFs) of the study area were weighted using the entropy approach. Lineament density, hydraulic conductivity, transverse resistance, transmissivity, and lithology make up the GPCFs studied. The result of the Python-based entropy weighting approach reveals that lineament density has the greatest impact on the groundwater potential of the study area, whereas hydraulic conductivity has the least weight and influence on groundwater storage potentiality. The PROMETHEE-II was then utilised to rank the alternatives using Python programming by calculating the net outranking flow of each alternative. The groundwater potential index (GPI) of the study area was computed using the net outranking flow. The PROMETHEE-Entropy model map of the study area was generated using the calculated GPI values in a GIS context. According to the groundwater potential model (GPM) map, 72% of the region has low groundwater potential, while the rest has medium to high groundwater potential. As a result, the aquifer units in the area are largely unproductive and have low groundwater potential.

The PROMETHEE-Entropy model map generated in Python was evaluated and compared using qualitative and quantitative validation methods. The qualitative validation was carried out using borehole pumping test data from the study area, and the PROMETHEE-Entropy success rate was 71%. The ROC curve was also used for quantitative validation, and the AUC for the PROMETHEE-Entropy method was 86%. The above validation findings indicate that the object-oriented PROMETHEE-Entropy-based groundwater potential model (GPM) is of good accuracy. The developed PROMETHEE-Entropy-based GPM tool may be used as part of a decision support system by water resource stakeholders to improve the development and management of groundwater resources in the investigated area and other places with similar geologic settings throughout the world.

Appendix

Entropy and PROMETHEE-II Python classes

```python
import numpy as np
import pandas as pd

df = pd.read_csv('Table 3.csv')
df_ = df.drop(['Fishnet no', 'Longitude', 'Latitude'], axis=1)
no_of_alt = 114
no_of_criteria = 5
matrix = df_.to_numpy()
types_ = np.array([1, 1, 1, 1, 1])
matrix


class Entropy_weight:

    def __init__(self, no_of_criteria, no_of_alt):
        self.no_of_criteria = no_of_criteria
        self.no_of_alt = no_of_alt


    def en_weight(self, matrix):
        summation_x_ij = matrix.sum(axis=0)
        matrix_df = pd.DataFrame(matrix)

        for i in range(self.no_of_criteria):
            matrix_df[i] = matrix_df[i] / summation_x_ij[i]

        normalized_list = np.array(matrix_df)
        normalized_df = pd.DataFrame(normalized_list, columns=
                        ['L', 'K', 'Ld', 'T', 'TR'])

        h = 1 / np.log(self.no_of_alt)
        log_df = np.log(pd.DataFrame(normalized_df))

        entropy_data = normalized_df.mul(log_df)
        entropy_j = -h * entropy_data.sum(axis = 0)

        dj = 1 - entropy_j
        dj_sum = dj.sum(axis=0)

        en_weight = dj/dj_sum

        return en_weight


class PROMETHEE_II:

    def __init__(self, no_of_criteria, no_of_alt, weights, types):
        self.no_of_criteria = no_of_criteria
        self.no_of_alt = no_of_alt
        self.weights = weights
        self.types = types


    def net_outranking_flow(self, matrix):

        m = pd.DataFrame(matrix)
        normalized_list = []

        for i in range(len(self.types)):
            if self.types[i] == -1:
                a = (max(m[i]) - m[i]) / (max(m[i]) - min(m[i]))
                normalized_list.append(a)
            elif self.types[i] == 1:
                b = (m[i] - min(m[i])) / (max(m[i]) - min(m[i]))
                normalized_list.append(b)
            else:
                pass

        normalized_df = pd.DataFrame(np.array(normalized_list).T)

        ith_list = []
```

```
for i in range(len(normalized_df.columns)):
    for k in range(self.no_of_alt):
        c = []
        for j in normalized_df[i]:
            a = normalized_df[i][k] - j
            c.append(a)
        ith_list.append(c)


ith_array = np.array(ith_list)
j = ith_array.ravel()

for i in range(len(j)):
    if j[i] <= 0:
        j[i] = 0

j.resize((self.no_of_criteria,int(self.no_of_alt * self.no_of_alt)))
ith_df = pd.DataFrame(j.T)

for i in range(len(self.weights)):
    ith_df[i] = ith_df[i] * self.weights[i]

aggregated_sum = ith_df.sum(axis = 1)
aggregated_sum_array = 
(aggregated_sum.to_numpy()).reshape(self.no_of_alt, self.no_of_alt)
aggregated_sum_df = pd.DataFrame(aggregated_sum_array)

neg_outflow_list = []
pos_outflow_list = []

for i in range(self.no_of_alt):
    negative_outflow = aggregated_sum_df[i].sum()/(self.no_of_alt -1)
    neg_outflow_list.append(negative_outflow)

    positive_outflow = aggregated_sum_df.iloc[i].sum() /
(self.no_of_alt - 1)

    pos_outflow_list.append(positive_outflow)

    net_outranking_flow = np.array(pos_outflow_list) -
np.array(neg_outflow_list)

return pd.DataFrame((np.array([pos_outflow_list,
                              neg_outflow_list,
                              net_outranking_flow]).T),
                    columns = ['Positive', 'Negative', 'Net'])

Entropy = Entropy_weight(no_of_criteria, no_of_alt)
Entropy.en_weight(matrix)


pro = PROMETHEE_II(no_of_criteria, no_of_alternatives, weights, types_)
pro.net_outranking_flow(matrix)
```

Declarations

Conflict of interest On behalf of all authors, the corresponding author states that there is no conflict of interest.

References

Abdullah L, Chan W, Afshari A (2019) Application of PROMETHEE method for green supplier selection: a comparative result based on preference functions. J Ind Eng Int 15:271–285. https://doi.org/10.1007/s40092-018-0289-z

Adeyemo IA, Omosuyi GO, Ojo BT, Adekunle A (2017) Groundwater potential evaluation in a typical basement complex environment using GRT index- a case study of Ipinsa-Okeodu area, near Akure, Nigeria. J Geosci Environ Prot 5:240–251

Adiat KAN, Nawawi MNM, Abdullah K (2012) Assessing the accuracy of GIS-based elementary multi-criteria decision analysis as a spatial prediction tool–a case of predicting potential zones of sustainable groundwater resources. J Hydrol 440–441:75–89

Adiat KAN, Nawawi MNM, Abdullah K (2013) Application of multi-criteria decision analysis to geoelectric and geologic parameters for spatial prediction of groundwater resources potential and aquifer evaluation. Pure Appl Geophys 170:453–471. https://doi.org/10.1007/s00024-012-0501-9

Adiat KAN, Ajayi OF, Akinlalu AA, Tijani IB (2019) Prediction of groundwater level in basement complex terrain using artificial neural network: A case of Ijebu-Jesa, southwestern Nigeria. Appl Water Sci 10(1):8. https://doi.org/10.1007/s13201-019-1094-6

Ajayi JO (2017) Water from Rocks, an inaugural lecture delivered at the Obafemi Awolowo University Press, Ile-Ife on 11th April, (2017). Inaugural lecture series press, Ile-ife 67p

Ajaykumar KK, Bhavana NU, Sankhua RN (2020) Assessment of recharge potential zones for groundwater development and management using geospatial and MCDA technologies in semiarid region of Western India. SN Appl Sci. https://doi.org/10.1007/s42452-020-2079-7

Akinlalu AA, Adegbuyiro A, Adiat KAN, Akeredolu BE, Lateef WY (2017) Application of multi-criteria decision analysis in prediction of groundwater resources potential: a case of Oke-Ana Ilesa area southwestern Nigeria. NRIAG J Astron Geophys 6:182–200

Akintorinwa OJ (2014) Groundwater potential assessment of Iwaro-Oka, SW Nigeria using geoelectric parameters. Br J Appl Sci Technol 6(4):364–377

Akintorinwa OJ, Atitebi MO, Akinlalu AA (2020) Hydrogeophysical and aquifer vulnerability zonation of a typical basement complex terrain: a case study of Odode Idanre southwestern Nigeria. Heliyon 6:e04549

Al-Abadi AM (2015) Groundwater potential mapping at northwestern Wasit and Missan governorates, Iraq using a data-driven weight of evidence technique in framework of GIS. Environ Earth Sci. https://doi.org/10.1007/s12665-015-4097-0

Al-Abadi AM, Shahid S (2016) Spatial mapping of artesian zone at Iraqi southern desert using a GIS-based random forest machine learning model. Model Earth Syst Environ 2:96

Al-Abadi AM, Pradhan B, Shahid S (2016) Prediction of groundwater flowing well zone at An-Najif province, central Iraq using evidential belief functions model and GIS. Environ Monit Assess 188:549. https://doi.org/10.1007/s10661-016-5564-0

Al-Abadi AM, Pourghasemi HR, Shahid S, Ghalib HB (2017) Spatial mapping of groundwater potential using entropy weighted linear aggregate novel approach and GIS. Arab J Sci Eng 42:1185–1199

Albadvi A, Chaharsooghi SK, Esfahanipour A (2007) Decision making in stock trading: an application of PROMETHEE. Eur J Oper Res 177:673–683

Alhassan DU, Obiora DN, Okeke FN (2015) The assessment of Aquifer potentials and aquifer vulnerability of southern Paiko, northcentral Nigeria, using geoelectric method. Global J Pure Appl Sci 21:51–70

Al-Sabahi E, Rahim SA, Wan Zahairi WY, Nozaily AI, Alshaebi F (2009) The characteristics of leachate and groundwater pollution at municipal solid waste landfill of Ibb City. Yemen Am J Environ Sci 5(3):256–266

Anbazhagan S, Balamurugan G, Biswal TK (2011) Remote sensing in delineating deep fracture aquifer zones. In: Anbazhagan S, Subramanian SK, Yang X (eds) Geoinformatics in applied geomorphology. CRC Press, Baco Raton, pp 205–229

Ariyo SO, Adeyemi GO (2009) Role of electrical resistivity method for groundwater exploration in hard rock areas: a case study from Fidiwo/Ajebo areas of Southwestern Nigeria. Pac J Sci Technol 10(1):483–486

Ariyo SO, Folorunso AF, Ajibade OM (2011) Geological and geophysical evaluation of the Ajana area's groundwater potential, Southwestern Nigeria. Earth Sci Res J 15(1):35–40

Arsène M, Wassouo Elvis BW, Daniel G, Théophile NM, Kelian K, Daniel NJ (2018) Hydrogeophysical investigation for groundwater resources from electrical resistivity tomography and self-potential data in the Meiganga area, Adamawa Cameroon. Int J Geophys. 14:2697585

Arshad A, Zhang Z, Zhang W, Dilawar A (2020) Mapping favorable groundwater potential recharge zones using a GIS-based analytical hierarchy process and probability frequency ratio model: a case study from an agro-urban region of Pakistan. Geosci Front 11(5):1805–1819

Ayşegül TI, Esra AA (2017) The decision-making approach based on the combination of entropy and Rov methods for the apple selection problem. Eur J Interdiscip Stud 3(3):80–86

Braga ACO, Dourado JC, Malagutti FW (2006) Resistivity (DC) method applied to aquifer protection studies. Braz J Geophys 24(4):573–581

Brans JP (1982) L'ingénièrie de la décision; Elaboration d'instruments d'aide à la décision. La méthode PROMETHEE. In R. Nadeau and M. Landry, editors, *L'aide à la décision: Nature, Instruments et Perspectives d'Avenir,* pages 183–213, Québec, Canada. Presses de l'Université Laval

Butwall M, Ranka P, Shah S (2019) Python in field of data science: a review. Int J Comput Appl 178(49):20–24. https://doi.org/10.5120/ijca2019919404

Chandra S, Ahmed A, Ram A, Dewandel B (2008) Estimation of hard rock aquifers hydraulic conductivity from geoelectrical measurements: a theoretical development with field application. J Hydrol 357:218–227. https://doi.org/10.1016/j.jhydrol.2008.05.023

Chen W, Li H, Hou E, Wang S, Wang G, Panahi M, Li T, Peng T, Guo C, Niu C, Xiao L, Wang J, Xie X, Ahmad BB (2018) GIS-based groundwater potential analysis using novel ensemble weights-of-evidence with logistic regression and functional tree models. Sci Total Environ 634:853–867. https://doi.org/10.1016/j.scitotenv.2018.04.055

Chowdhury A, Jha MK, Chowdary VM, Mal BC (2009) Integrated remote sensing and GIS-based approach for assessing groundwater potential in West Medinipur district, West Bengal India. Int J Remote Sens 30(1):231–250

CorsiniCerviRonchetti AFF (2009) Weight of evidence and artificial neural networks for potential groundwater spring mapping: an application to the Mt Modino area Northern Apennines Italy. Geomorphology 111:79–87

Diminescu MA, Dumitran GE, Vuta LL (2019) Experimental methods to determine the hydraulic conductivity (2019). Dio: https://doi.org/10.1051/e3sconf/20198506010

Duze M, Ojo A (1982) Senior school atlas. Macmillian Education, Lagos. pp 113

El-mahdy SI, Mohamed MM (2014) Groundwater potential modeling using remote sensing and GIS: a case study of the Al Dhaid area. United Arab Emirates Geocarto Int. https://doi.org/10.1080/10106049.2013.784366

Jenks GF (1967) The data model concept in statistical mapping. Int Yearb Cartograp 7:973–980

Karnieli A, Meisels A, Fisher L (1996) Automatic extraction and evaluation of geological linear features from digital remote sensing data using a hough transform. Photogramm Eng Remote Sens 62(5):525–531

Lee S, Kim YS, Oh HJ (2012) Application of a weights-of-evidence method and GIS to regional groundwater productivity potential mapping. J Environ Manag 96(1):91–105

Li P, Wu J, Qian H (2012) Groundwater quality assessment based on rough sets attribute reduction and TOPSIS method in a semi-arid area. China Environ Monit Assess 184:4841–4854. https://doi.org/10.1007/s10661-011-2306-1

Lin ZZ, Wen FS (2009) Entropy weight-based decision-making theory and its application to black-start decision-making. Proceedings of the CSU EPSA 21(6):26–33

Manap MA, Nampak H, Pradhan B, Lee S, Sulaiman WNA, Ramli MF (2014) Application of probabilistic-based frequency ratio model in groundwater potential mapping using remote sensing data and GIS. Arab J Geosci 7:711–724

McKay G, Harris JR (2015) Comparison of the data-driven random forests model a knowledge-driven method for mineral prospectivity mapping: a case study for gold deposits around the Huritz Group and Nueltin Suite, Nunavut. Canada Nat Resour Res. https://doi.org/10.1007/s11053-015-9274-z

Mogaji KA (2016) Combining geophysical techniques and multi-criteria GIS-based application modeling approach for groundwater potential assessment in southwestern Nigeria. Environ Earth Sci. https://doi.org/10.1007/s12665-016-5897-6

Mogaji KA, Lim HS (2016) Groundwater potentiality mapping using geoelectrical-based aquifer hydraulic parameters: GIS-based multi-criteria decision analysis modeling approach. Terr Atmos Ocean Sci. https://doi.org/10.3316/TAO.2016.11.01.02

Mogaji KA, Lim HS (2019) A GIS-based linear regression modeling approach to assess the impact of geologic rock types on groundwater recharge and its hydrological implication. Model Earth Syst Environ. https://doi.org/10.1007/s40808-019-00670-3

Mogaji KA, Omobude OB (2017) Modeling of geoelectric parameters for assessing groundwater potentiality in a multifaceted geologic terrain, Ipinsa Southwest, Nigeria- A GIS-based GODT approach. J Astron Geophys 6:434–451

Mogaji KA, Olayanju GM, Oladapo MI (2011) Geophysical evaluation of rock type impact on aquifer characterization, geo-electric assessment and GIS approach in the basement complex of Ondo state, southwestern Nigeria. Int J Water Resourc Environ Eng 3(4):77–86

Mogaji KA, Lim HS, Abdullah K (2014) Regional prediction of groundwater potential mapping in a multifaceted geology terrain using GIS-based Dempster-Shafer model. Arab J Geosci 8(5):1–24

Mogaji KA, Lim HS, Abdullah K (2015) Modeling groundwater vulnerability prediction using geographic information system (GIS)-based ordered weighted average (OWA) method and DRASTIC model theory hybrid approach. Arab J Geosci. https://doi.org/10.1007/s12517-013-1163-3

Mogaji KA, Gbode IE, Olayanju OA (2021) Modeling of aquifer potentiality using GIS-based knowledge driven technique: a case study of hard rock geological setting, southwestern Nigeria. Sustain Water Resour Manag 7:64. https://doi.org/10.1007/s40899-021-00538-4

Molden D (2007) Water for food, water for life: a comprehensive assessment of water management in agriculture. Earth scan/IWMI

Mostafa ME, Zakir FA (1996) New enhancement techniques for azimuthal analysis of lineaments for detecting tectonic trends in and around the Afro-Arabian shield. Int J Remote Sens 17:2923–2943

Naghibi SA, Pourghasemi HA, Pourtaghi Z, Rezaei A (2014) Groundwater qanat potential mapping using frequency ratio and Shannon's entropy models in the Moghan watershed. Iran Earth Sci Inform. https://doi.org/10.1007/s12145-014-0145-7

Nampak H, Pradhan B, Manap MA (2014) Application of GIS-based data driven evidential belief function model to predict groundwater potential zonation. J Hydrol 513:283–300

Nasiri H, Boloorani AD, Sabokbar HAF, Jafari HR, Hamzeh M, Rafii Y (2012) Determining the most suitable areas for artificial groundwater recharge via an integrated PROMETHEE II-AHP method in GIS environment (case study: Garabaygan Basin, Iran). Environ Monit Assess. https://doi.org/10.1007/s10661-012-2586-0

Nigeria Geological Survey Agency (NGSA) (2006) Published by the Authority of the Federal Republic of Nigeria

Obaje NG (2009) Geology and mineral resources of Nigeria. Springer, Berlin, p 221. https://doi.org/10.1007/978-3-540-92685-6

Odeyemi IB, Malomo S, Okufarasin YA (1985) Remote sensing of rock fractures and groundwater development success in parts of Southwestern Nigeria. In: Natural Resources Forum, United Nations, New York

Oh HJ, Kim YS, Choi JK, Park E, Lee S (2011) GIS mapping of regional probabilistic groundwater potential in the area of Pohang City. Korea J Hydrol 399:158–172. https://doi.org/10.1016/j.jhydrol.2010.12.027

Okogbue CO, Omonona OV (2013) Groundwater potential of the Egbe-Mopa basement area, central Nigeria. Hydrol Sci J. https://doi.org/10.1080/02626667.2013.775445

Olabode OF (2019) Potential groundwater recharge sites mapping in a typical basement terrain: a GIS methodology approach. J Geovis Spat Anal. https://doi.org/10.1007/s41651-019-0028-z

Oladunjoye MA, Korode IA, Adefehinti A (2019) Geoelectrical exploration for groundwater in crystalline basement rocks of Gbongudu community, Ibadan, southwestern Nigeria. Global J Geol Sci 17:25–43

Oleary DW, Friedman JD, Phn HA (1976) Lineament, linear, lineation: some proposed new standard for old terms. Geol Soc Amer Bull 87:1463–1469

Olorunfemi MO (1990) The Hydrogeological Implication of Topographic Variation with Overburden Thickness in Basement Complex Area of Southwestern Nigeria. J min Geol 26(1)

Omosuyi GO (2010) Geoelectric assessment of groundwater prospect and vulnerability of overburden aquifers at Idanre, southwestern Nigeria. Ozean J App Sci 3(1):19–28

Ouedraogo I, Defourny P, Vanclooster M (2016) Mapping the groundwater vulnerability for pollution at the pan-African scale. Sci Total Environ 544:939–953

Oyedotun TDT, Obatoyinbo O (2012) Hydro-geochemical evaluation of groundwater quality in Akoko NorthWest local government area of Ondo State. Nigeria Revista Ambiente & Agua 7(1):67–80

Ozdemir A (2011) Using a binary logistic regression method and GIS for evaluating and mapping the groundwater spring potential in the Sultan Mountains (Aksehir, Turkey). J Hydrol 405(1):123–136

Pourghasemi HR, Beheshtirad M (2015) Assessment of data-driven evidential belief function model and GIS for groundwater potential mapping in the Koohrang Watershed. Iran Geocarto International 30(6):662–685. https://doi.org/10.1080/10106049.2014.966161

Pourtaghi ZS, Pourghasemi HR (2014) GIS-based groundwater spring potential assessment and mapping in the Birjand Township, southern Khorasan Province Iran. Hydrogeol J 22(3):643–662

Qi Y, Wen F, Wang K, Li L, Singh SN (2010) A fuzzy comprehensive evaluation and entropy weight decision-making based method for power network structure assessment. Int J Eng Sci Technol 2(5):92–99

Rahaman MA (1988) Recent advances in the study of the basement complex of Nigeria. In: Geological Survey of Nigeria (Ed) Precambrian Geology Nigeria, 11–43 pp

Rahmati O, Meselle AM (2016) Application of Dempster-Shafer theory, spatial analysis and remote sensing for groundwater potentiality and nitrate pollution analysis in the semi-arid region of Khuzestan Iran. Sci Total Environ 568:1110–1123

Rahmati O, Nazari SA, Mahdavi M, Pourghasemi HR, Zeinivand H (2015) Groundwater potential mapping at Kurdistan region of Iran using analytic hierarchy process and GIS. Arab J Geosci 8:7059–7071

Roodposhti MS, Rahimi S, Beglou MJ (2012) PROMETHEE II and fuzzy AHP: an enhanced GIS-based landslide susceptibility mapping. Nat Hazards. https://doi.org/10.1007/s11069-012-0523-8

Saaty RW (1987) The analytical hierarchy process – the analytical hierarchy process – what it is and how it is used. Pergamon J Ltd 9(3–5):161–176

Safari H, Fagheyi MS, Ahangari SS, Fathi MR (2012) Applying Promethee method based on entropy weight for supplier selection. Bus Manag Strategy 3(1):97–106

Salem HS (1999) Determination of fluid transmissivity and electric transverse resistance for shallow aquifers and deep reservoirs from surface and well-log electric measurements. Hydrol Earth Syst Sci 3:421–427. https://doi.org/10.5194/hess-3-421-1999

Shannon CE (1948) A mathematical theory of communications. Bell Syst Tech J 27(3):379–423

Srinivasan V, Thomas BK, Jamwal P, Lele S (2013) Climate vulnerability and adaptation of water provisioning in developing countries: approaches to disciplinary and research-practice integration. Curr Opin Environ Sustain 5:1–6. https://doi.org/10.1016/j.cosust.2013.07.011

Tizro AT, Voudouris KS, Salehzade M, Mashayekhi H (2010) Hydrogeological framework and estimation of aquifer hydraulic parameters using geoelectrical data: a case study from West Iran. Hydrogeol J 18(4):917–929

Vander-Velper BPA. (2004) WinRESIST Version 1.0 Resistivity Depth Sounding Interpretation Software M.Sc. Research Project. ITC, Delft Netherland

Vincke JP, Brans P (1985) A preference ranking organization method The PROMETHEE method for MCDM. Manag Sci 31:641–656

Wang B, Teng Y, Wang H, Zuo R, Zhai Y, Weifeng Y, Yang J (2020) Entropy weight method coupled with an improved DRASTIC model evaluate the special vulnerability of groundwater in Songnen Plain Northeastern China. Hydrol Res 51(5):1184–1200

Widianta MMD, Rizaldi T, Setyohadi DPS, Riskiawan HY (2018) Comparison of Multi-Criteria Decision Support Methods (AHP, TOPSIS, SAW & PROMETHEE) for Employee Placement. J Phys Conf Ser 953:012116

Yousefi H, Zahedi S, Niksokhan MK (2018) Modifying the analysis made by water quality index using multi-criteria decision-making methods. J Afr Earth Sc 138:309–318

Zakir FA, Mohammed HT, Qari ME (1999) A new optimizing technique for preparing lineament density maps. Int J Remote Sens 20(6):1073–1085

Zare M, Pourghasemi HR, Vafakhah M, Pradhan B (2013) Landslide susceptibility mapping at Vaz Watershed (Iran) using an artificial neural network model: a comparison between multilayer perceptron (MLP) and radial basic function (RBF) algorithms. Arab J Geosci 6:2873–2888

Zou Z, Yun Y, Sun J (2006) Entropy method for determination of the weight of evaluating indicators in fuzzy synthetic evaluation for water quality assessment. J Environ Sci 18(5):1020–1023